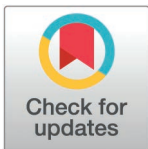


RESEARCH ARTICLE

A phage-encoded counter-defense inhibits an NAD-degrading anti-phage defense system

Christian L. Loyo , Alan D. Grossman *

Department of Biology, Massachusetts Institute of Technology, Cambridge, Massachusetts, United States of America

* adg@mit.edu

Abstract

Bacteria contain a diverse array of genes that provide defense against predation by phages. Anti-phage defense genes are frequently located on mobile genetic elements and spread through horizontal gene transfer. Despite the many anti-phage defense systems that have been identified, less is known about how phages overcome the defenses employed by bacteria. The integrative and conjugative element ICEBs1 in *Bacillus subtilis* contains a gene, *spbK*, that confers defense against the temperate phage SPβ through an abortive infection mechanism. Using genetic and biochemical analyses, we found that SpbK is an NADase that is activated by binding to the SPβ phage portal protein YonE. The presence of YonE stimulates NADase activity of the TIR domain of SpbK and causes cell death. We also found that the SPβ-like phage Φ3T has a counter-defense gene that prevents SpbK-mediated abortive infection and enables the phage to produce viable progeny, even in cells expressing *spbK*. We made SPβ-Φ3T hybrid phages that were resistant to SpbK-mediated defense and identified a single gene in Φ3T (*phi3T_120*, now called *nip* for NADase inhibitor from phage) that was both necessary and sufficient to block SpbK-mediated anti-phage defense. We found that Nip binds to the TIR (NADase) domain of SpbK and inhibits NADase activity. Our results provide insight into how phages overcome bacterial immunity by inhibiting enzymatic activity of an anti-phage defense protein.

OPEN ACCESS

Citation: Loyo CL, Grossman AD (2025) A phage-encoded counter-defense inhibits an NAD-degrading anti-phage defense system. *PLoS Genet* 21(4): e1011551. <https://doi.org/10.1371/journal.pgen.1011551>

Editor: Aimee Shen, Tufts University School of Medicine, UNITED STATES OF AMERICA

Received: December 20, 2024

Accepted: March 10, 2025

Published: April 2, 2025

Copyright: © 2025 Loyo. This is an open access article distributed under the terms of the [Creative Commons Attribution License](https://creativecommons.org/licenses/by/4.0/), which permits unrestricted use, distribution, and reproduction in any medium, provided the original author and source are credited.

Data availability statement: The authors confirm that all data underlying the findings are fully available without restriction. All relevant data are within the paper and its [Supporting Information](#) files.

Funding: Research reported here is based upon work supported, in part, by the National Institute of General Medical Sciences and the National Institutes of Health under award number R35 GM122538 and R35 GM148343

Author summary

Bacterial viruses (bacteriophages or phages) are widespread and abundant across the planet. Bacteria have a variety of immune systems, often found on mobile genetic elements, to combat phage predation. Phages can overcome these immune systems by mutating to avoid recognition or by producing molecules that prevent the immune system from working. We determined how an anti-phage defense system encoded by an integrative and conjugative element recognizes phage infection to cause cell death prior to the generation of phage progeny. We also identified a phage gene that prevents this defense system from functioning. The phage-encoded counter-defense protein inhibits the enzymatic activity of the anti-phage defense protein, enabling evasion of immunity and production of infectious phage. Our findings highlight the evolving interactions between bacteria and phages.

to ADG. CLL was supported, in part, by the NIGMS predoctoral training grant T32 GM007287. The funders had no role in study design, data collection and analysis, decision to publish, or preparation of the manuscript.

Competing interests: The authors have declared that no competing interests exist.

Introduction

Bacteria have many different types of immune systems that protect against bacteriophages (phages). These anti-phage defense systems work through a variety of different mechanisms to limit the spread of phages. Many anti-phage defense systems work through abortive infection, wherein the phage and cell are both destroyed during the course of infection, preventing phage propagation within a population of cells [1]. Phages can have counter-defense genes that enable the phage to circumvent one or more anti-phage defense systems. These phage-encoded counter-defenses are diverse in how they enable evasion of the host-mediated defense, including blocking recognition of phage infection by the defense system and inhibiting the enzymatic activity of anti-phage defense proteins [2].

Bacteria typically contain several mobile genetic elements, including plasmids, temperate phages, and integrative and conjugative elements (ICEs). Anti-phage defense genes are often found on mobile genetic elements as part of the repertoire of so-called cargo genes. Cargo genes are not required for the lifecycle of a mobile element but often confer some benefit to their host. Because of their ability to move from host to host, mobile genetic elements that contain anti-phage defense genes facilitate rapid adaptation to phage infection and acquisition [3].

Many isolates of *Bacillus subtilis* harbor the integrative and conjugative element ICEBs1 [4]. The product of the ICEBs1 gene *spbK* prevents propagation of the phage SP β through an abortive infection mechanism that is activated by the phage protein YonE [5]. *yonE* was initially identified in a Tn-seq screen to identify host mutants that affect receipt of ICEBs1 during conjugation [5,6]. The screen identified a mutant with a transposon insertion in the temperate phage SP β , upstream of *yonE* in the lysogen. This insertion drove erroneous expression of *yonE* while SP β was in the prophage state. It was subsequently determined that expression of *yonE* and *spbK*, even in the absence of any other genes in SP β or ICEBs1, causes cell death [5].

yonE is essential for production of functional phage [5] and its product is predicted to be the phage portal protein that is needed for DNA packaging into the capsid and subsequent extrusion of DNA from the capsid into the tail during infection [7,8]. SpbK is not required for the ICEBs1 lifecycle [5]. It contains a toll-interleukin-1 receptor-like (TIR) domain (Fig 1A and 1B) that is found in several proteins in both prokaryotes and eukaryotes [9,10], many of which have NADase activity [11].

Here, we report that SpbK is an NADase that is activated by the phage portal protein YonE to cause depletion of NAD⁺ during infection. We also found that the SP β -like phage Φ 3T is resistant to SpbK-mediated abortive infection and identified a single gene in Φ 3T, *phi3T_120* (now called *nip*, for NADase inhibitor from phage), that was both necessary and sufficient for this counter-defense. We found that Nip bound to the TIR (NADase) domain of SpbK and inhibited its NADase activity, preventing abortive infection and enabling the phage to grow and propagate.

Results

The anti-phage defense protein SpbK is an NADase that is activated by the SP β phage portal protein YonE

Because many proteins that contain a TIR domain are NADases, we decided to test if SpbK had NADase activity in vivo, and if that activity was stimulated by the phage protein YonE. We measured NAD⁺ levels in cells expressing *spbK* with and without expression of *yonE*. *spbK* was expressed from its own promoter from ICEBs1 and *yonE* was expressed from the IPTG-inducible promoter Pspank(hy) {Pspank(hy)-*yonE*}. Expression of *yonE* alone had no detectable effect on growth (Fig 1C and 1D), as previously determined [5], and no detectable effect

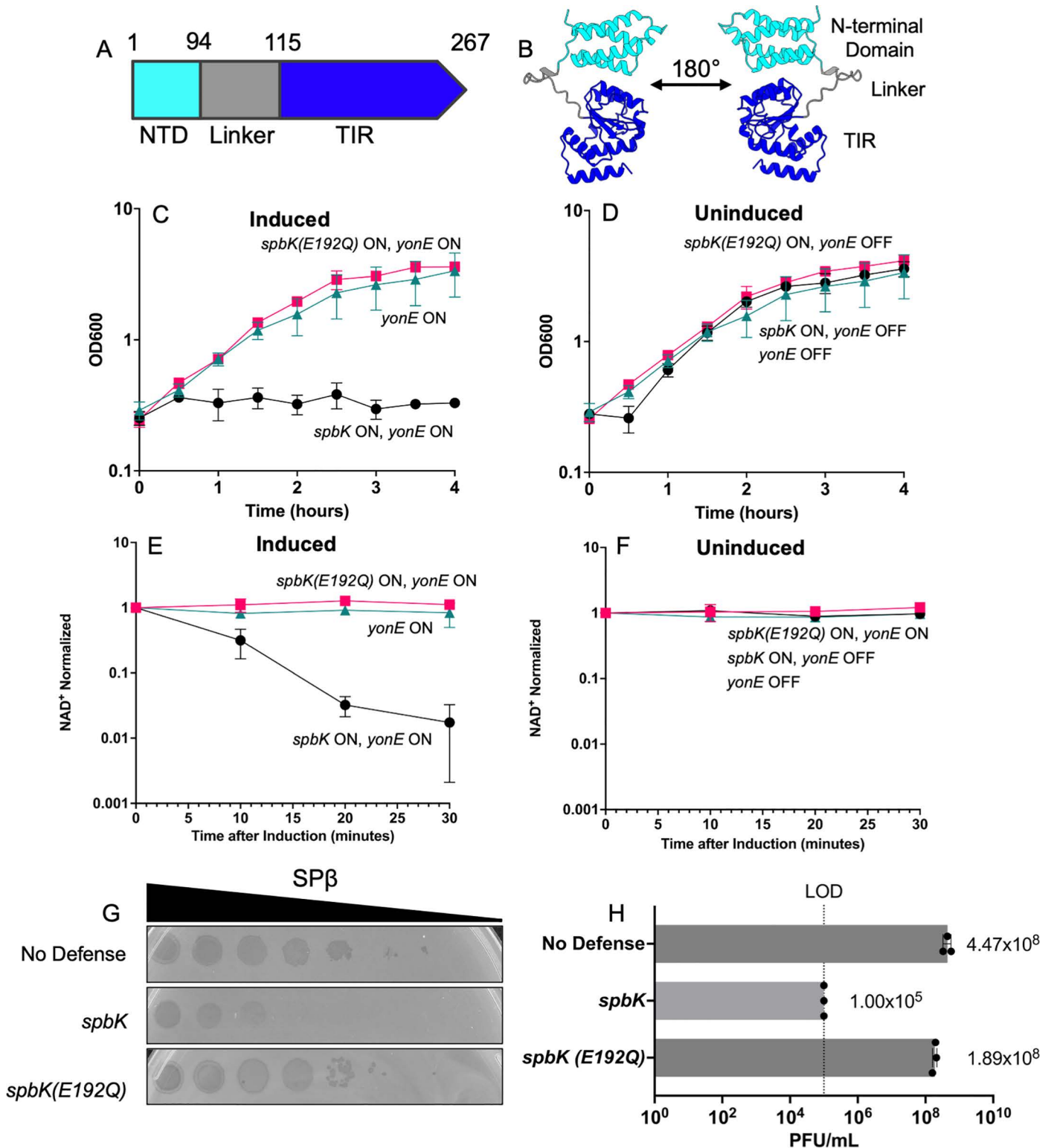


Fig 1. SpbK is an NADase that is activated by the phage protein YonE. A) Predicted domain architecture of SpbK. SpbK is 267 amino acids and includes the N-terminal domain (cyan; aa 1-94), the linker domain (aa 95-115), and the Toll-interleukin-1 receptor (TIR) domain (dark blue; aa 116-267). B) AlphaFold3 model of a monomer of SpbK. The N-terminal domain is colored in cyan, the linker domain is colored in gray, and the Toll-interleukin-1 receptor (TIR) domain in dark blue. The predicted template modeling score (pTM) is 0.62 and the mean predicted local distance test (pLDDT) score is 95.53, indicating high confidence in the predictions. C, D, E, F) Strains co-expressing *spbK* and *yonE* (CMJ685, black circles), *spbK(E192Q)* and *yonE* (CLL317, pink squares), or only *yonE*

(CMJ616, turquoise triangles) were grown in $S7_{50}$ minimal medium. Expression of Pspank(hy)-*yonE* was induced with 1 mM IPTG. Culture turbidity (C, D) and levels of NAD^+ (E, F) were measured over time. Levels of NAD^+ were normalized to the amount of NAD^+ per OD 0.025 cells at $T=0$. Measurements at $T=0$ were taken immediately before addition of IPTG. Error bars represent standard deviation and are not always visible. G) Ten-fold serial dilutions of SP β phage were spotted onto isogenic strains expressing no anti-phage defense (CU1050, top row), *spbK* (CMJ534, middle row), or *spbK(E192Q)* (CLL164, bottom row). Large zones of clearing are indicative of a confluence of phage plaques and cell lysis. Small zones of clearing are indicative of individual or small clusters of phage plaques. H) *spbK(E192Q)* is not functional in phage defense. The ability of SP β to grow (make plaques) on cells with no anti-phage defense (CU1050, top bar), *spbK* (CMJ534, middle bar), or *spbK(E192Q)* (CLL164, bottom bar) was determined. PFU/ml from three independent experiments is shown. The limit of detection in these experiments was $\sim 10^5$ PFU/ml. Error bars represent standard deviation and are not always visible due to the size of the data point.

<https://doi.org/10.1371/journal.pgen.1011551.g001>

on cellular levels of NAD^+ (Fig 1E and 1F). Cells expressing *spbK* (from its own promoter), without induction of Pspank(hy)-*yonE*, grew normally (Fig 1D) and had normal levels of NAD^+ (Fig 1F). In marked contrast, induction of *yonE* in cells expressing *spbK* caused growth arrest (Fig 1C), as previously described [5], and a drop in levels of NAD^+ (Fig 1E). By 15 minutes after inducing expression of *yonE* by addition of IPTG, there was an approximate 10-fold drop, and by 30 minutes there was an approximately 100-fold drop in levels of NAD^+ (Fig 1E). We note that co-expression of *spbK* and *yonE* causes an ~ 10 -fold drop in viability (as measured by the ability to form colonies) by 30 minutes after induction of Pspank(hy)-*yonE* [5].

TIR-domain containing proteins that act as NADases have a conserved glutamate in the active site that is required for cleavage of NAD^+ [10–12]. We used DALI to identify proteins with that are structurally similar to SpbK and found that many are TIR-domain containing proteins that act as NADases, including AbTIR (S1A and S1B Fig) and TIR-APAZ (S1C and S1D Fig), proteins that are known to be NADases [11,13,14]. A multiple sequence alignment of SpbK to similar proteins also indicated that a highly conserved glutamate at position 192 (Glu192) of SpbK was likely to be in the catalytic site (S1E Fig). We changed Glu192 to glutamine (E192Q) and tested for effects on cell growth (Fig 1C and 1D), levels of NAD^+ (Fig 1E and 1F), and anti-phage defense (Fig 1G and 1H). The *spbK(E192Q)* mutation abolished anti-phage defense (Fig 1G and 1H). That is, SP β was able to grow and make plaques and had an increase in phage titers on cells expressing the mutant *spbK*, in contrast to the absence of phage growth in cells expressing wild type *spbK* (Fig 1G and 1H). In contrast to the results with co-expression of *yonE* with wild type *spbK* (Fig 1C), co-expression of *yonE* with *spbK(E192Q)* caused no detectable change in cell growth (Fig 1C) and no decrease in the amount of NAD^+ (Fig 1E), indicating that both of these phenotypes are dependent on the activity of the TIR domain in SpbK. Together, these results indicate that SpbK acts as a NADase and is activated by the SP β phage portal protein YonE.

SpbK and YonE interact directly

We tested for interaction between SpbK and YonE using immunoprecipitation of epitope-tagged proteins. We fused a FLAG tag to the N-terminus of SpbK (FLAG-SpbK) and a 3xMyc tag to the C-terminus of YonE (YonE-Myc). Both fusion proteins were functional (S2 Fig): FLAG-SpbK inhibited growth of SP β (S2A Fig) and expression of YonE-Myc caused growth arrest in cells also expressing SpbK (S2B Fig).

We found that SpbK and YonE interact directly *in vivo*. We co-expressed FLAG-SpbK (from the *spbK* promoter; Methods) and YonE-Myc (from Pspank(hy); Methods) in the absence of any other genes from *ICEBs1* or SP β , immunoprecipitated FLAG-SpbK with anti-FLAG antibodies, ran the samples on SDS polyacrylamide gels, and probed Western blots for YonE-Myc using anti-c-Myc antibodies. We found that YonE-Myc co-precipitated with FLAG-SpbK (Fig 2A, lane 4). In control experiments in which we expressed SpbK (no tag) with YonE-Myc or FLAG-SpbK with YonE (no tag), we no longer detected YonE-myc in Western blots of immunoprecipitated material (Fig 2A, lanes 2 and 3). These controls indicate

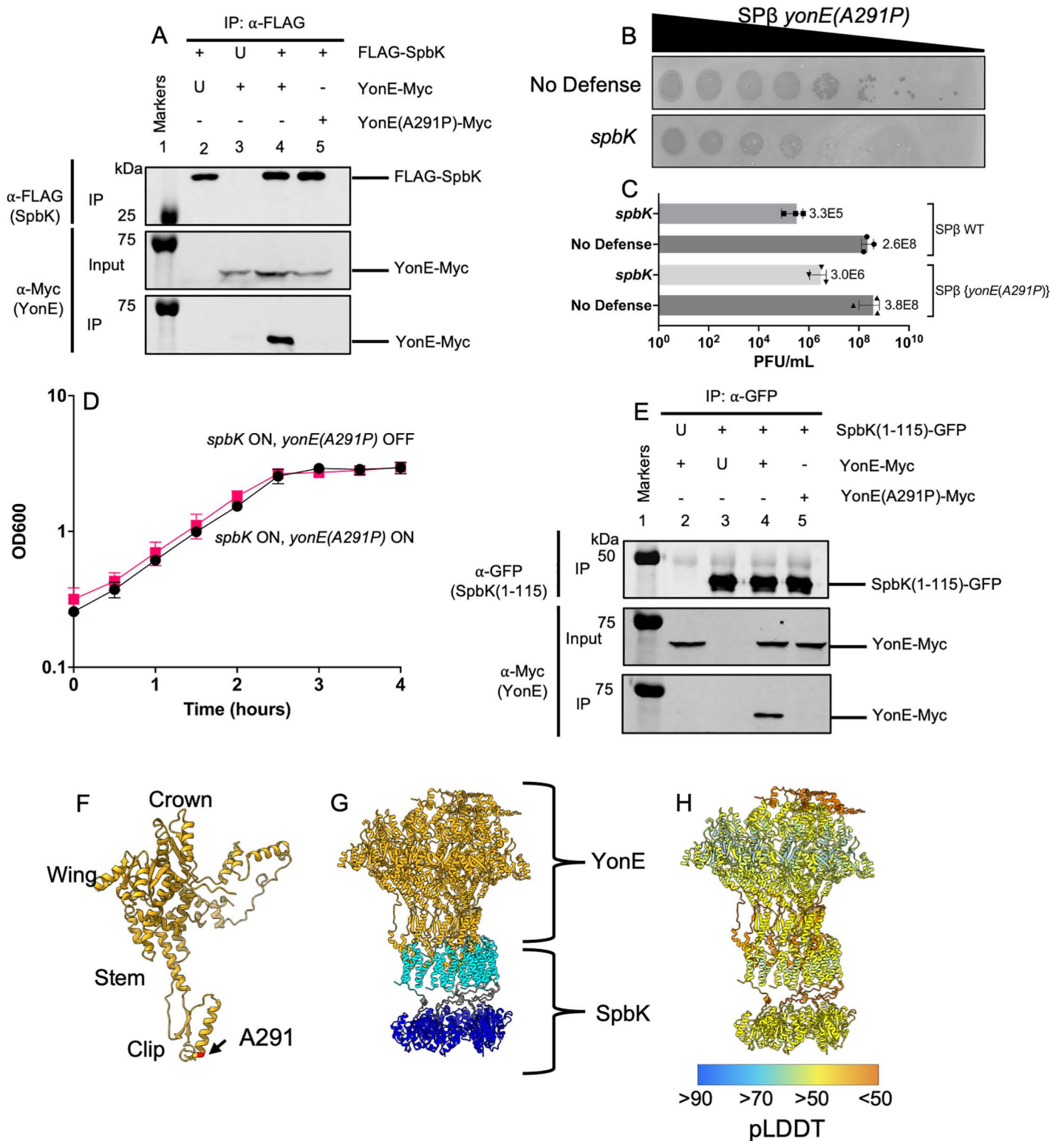


Fig 2. The N-terminal domain of SpbK interacts with the clip domain of YonE. In the immunoprecipitation experiments (A, E), the indicated proteins were produced in cells without ICEBs1 or SP β . A) SpbK interacts with YonE. Co-immunoprecipitation experiments to probe interactions between FLAG-SpbK and YonE-Myc or YonE(A291P)-Myc. Top row: Western blot probed with α -FLAG monoclonal antibody on IP fractions. Second row: Western blot probed with α -c-Myc monoclonal antibody on input fractions. Third row: Western blot probed with α -c-Myc monoclonal antibody on IP fractions. Lane 1 contains molecular weight markers from the Odyssey One-Color Protein Molecular Weight Marker Ladder (LI-COR). Lysates from the following strains were used for immunoprecipitations:

CLL609 (lane 2), CLL334 (lane 3), CLL373 (lane 4), and CLL615 (lane 5). Data shown are representative of three biological replicates. U, untagged protein expressed; +, tagged protein expressed; -, protein not expressed. **B, C**) Escape of SpbK-mediated defense by SPβ *yonE(A291P)*. **B**) Spot assays with ten-fold dilutions of SPβ *yonE(A291P)* spotted onto isogenic strains with no phage defense (CU1050, top row) or expressing *spbK* (CMJ534, bottom row). Large zones of clearing are indicative of a confluence of phage plaques and cell lysis. Small zones of clearing are indicative of individual or small clusters of phage plaques. **C**) Lysogens of SPβ (top two bars) in cells with no defense (CLL118, top bar) or with *spbK* (CLL452, second bar) and SPβ *yonE(A291P)* (bottom two rows) with no defense (CLL453; third bar) or with *spbK* (CLL466; fourth bar) were induced by addition of mitomycin C (1 μg/ml) to growing cells. PFUs/ml were determined on strain CU1050. Error bars represent standard deviation and are not always visible due to the size of the data point. **D**) Expression of *yonE(A291P)* does not activate SpbK-mediated growth arrest. Strains co-expressing *spbK* and *yonE(A291P)* were grown in S_{750} minimal medium and growth was monitored by OD₆₀₀ for 4 hours. *yonE(A291P)* was induced with 1mM IPTG (black circles) or left uninduced (pink squares). Measurements at T=0 were taken immediately before addition of IPTG. Data shown are from three biological replicates. Error bars represent standard deviation and are not always depicted due to the size of the data point. **E**) The N-terminal domain of SpbK interacts with YonE, but not YonE(A291P). Co-immunoprecipitation experiments to probe interactions between SpbK(1-115)-GFP and YonE-Myc or YonE(A291P)-Myc. Top row: Western blot probed with α-GFP polyclonal antibody on IP fractions. Second row: Western blot probed with α-c-Myc monoclonal antibody on input fractions. Third row: Western blot probed with α-c-Myc monoclonal antibody on IP fractions. Lane 1 contains molecular weight markers from the Odyssey One-Color Protein Molecular Weight Marker Ladder (LI-COR). Lysates from the following strains were used for immunoprecipitations: CLL718 (lane 2), CLL719 (lane 3), CLL720 (lane 4), and CLL721 (lane 5). Data shown are representative of three biological replicates. U, untagged protein expressed; +, tagged protein expressed; -, protein not expressed. **F**) Alanine 291 is located in the clip domain of YonE. A monomer of the YonE portal protein was modeled using AlphaFold3. The approximate location of the clip, stem, wing, and crown domains are labeled. The location of the A291P mutation is highlighted in red. The pTM score is 0.75 and the mean pLDDT score is 77.91, indicating moderate confidence in the predictions. **G**) The N-terminal domain of SpbK is predicted to interact with the clip domain of YonE. Six units of YonE (gold) were modeled with six units of SpbK using AlphaFold3. The N-terminal region of SpbK is colored cyan, the linker region of SpbK is colored gray, and the TIR domain of SpbK is colored dark blue. The pTM score is 0.47, the mean pLDDT score is 67.77, and the interface predicted template modeling (ipTM) score is 0.43, indicating low confidence in the specific molecular interactions. **H**) AlphaFold3 model shown in **G** with residues colored by pLDDT score.

<https://doi.org/10.1371/journal.pgen.1011551.g002>

that the anti-FLAG antibodies were specifically immunoprecipitating FLAG-SpbK and the anti-Myc antibodies were specifically detecting YonE-Myc. Further, the presence of YonE-Myc in the IP fraction was dependent on FLAG-SpbK, as we detected YonE-Myc in input samples (whole cell lysates) but only detected YonE-Myc in the immunoprecipitates when FLAG-SpbK was also present (Fig 2A, lanes 2 and 3). Together, these results indicate that SpbK and YonE are likely interacting directly, and that this interaction does not require any other ICEBs1 or SPβ products. Although we have no evidence, we cannot rule out the formal possibility that a host factor is also involved in this interaction.

Because YonE from SPβ activates SpbK to cause abortive infection and prevent phage growth [5], we sought to isolate phage mutants that escape the SpbK-mediated anti-phage defense. These phage mutants should be able to grow and make plaques on cells producing SpbK. We isolated one such mutant from a population of approximately 10¹⁰ phage (Fig 2B). This phage had a mutation in *yonE* that changed alanine at position 291 to proline {*yonE(A291P)*}. Relative to that of the wild type phage, the SPβ *yonE(A291P)* mutant had ~10-fold increased plaquing efficiency on cells expressing *spbK*, although it did not fully escape SpbK-mediated defense (Fig 2B). Further, we tested the ability of SPβ *yonE(A291P)* to escape *spbK* when induced from a prophage state. Similar to what was observed with the spot dilution assay, SPβ *yonE(A291P)* produced ~10-fold more phage in cells expressing *spbK* than wild type SPβ in cells expressing *spbK* (Fig 2C). Expression of the mutant *yonE* allele did not cause growth arrest when co-expressed with *spbK* (Fig 2D), indicating that YonE(A291P) might not interact with or has a weaker interaction with SpbK than wild type YonE when expressed outside the context of phage infection.

We used immunoprecipitation to test for interaction between SpbK and the YonE(A291P) mutant. As above, we expressed FLAG-SpbK and YonE(A291P)-Myc and immunoprecipitated FLAG-SpbK. We did not detect YonE(A291P)-Myc in the immunoprecipitates as determined by Western blot (Fig 2A, lane 5), indicating that if SpbK interacts with the mutant YonE, then this interaction is below the limit of detection of the immunoprecipitations. Because the *yonE(A291P)* mutant phage do not fully escape SpbK-mediated defense, we suspect that the mutant YonE is capable of weakly activating the defense and reducing phage production. It is also formally possible that there is another phage protein that activates SpbK,

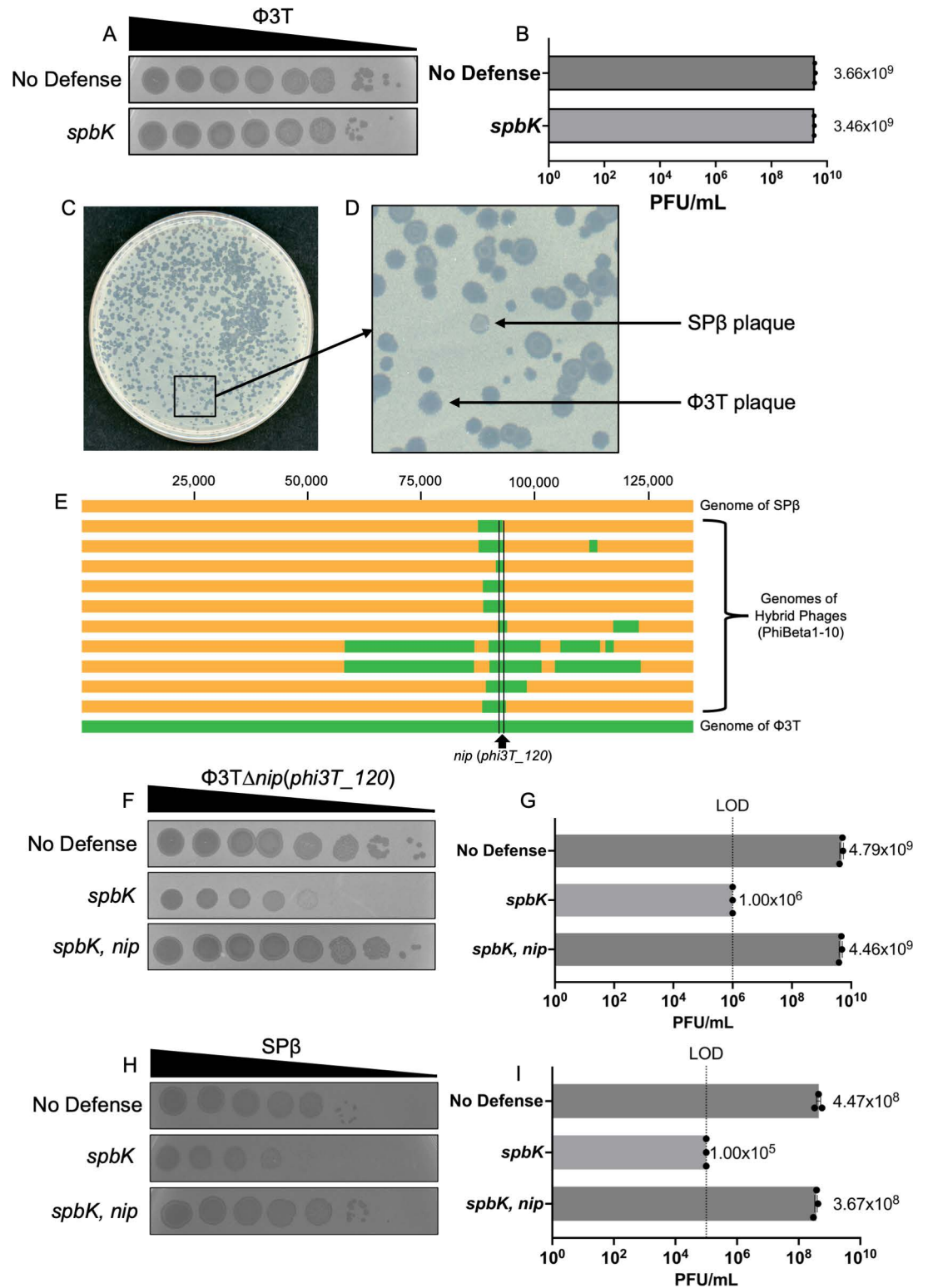


Fig 3. Phage Φ 3T encodes a counter-defense against SpbK-mediated phage defense. A) Φ 3T escapes SpbK-mediated phage defense. Ten-fold dilutions of Φ 3T was spotted onto isogenic strains without anti-phage defense (CU1050; top row) or expressing *spbK* (CMJ534; bottom row). Large zones of clearing are indicative of a confluence of phage plaques and cell lysis. Small zones of clearing are indicative of individual or small clusters of phage plaques. B. Φ 3T phage grows similarly on strains with no anti-phage defense (CU1050, top bar) or *spbK* (CMJ534, bottom bar). Error bars represent standard deviation and are

not always visible due to the size of the data point. **C**) Plaques formed on a plate with strain expressing *spbK*. Double lysogens of $\Phi 3T$ and SP β c2 were treated with heat shock (methods). Phages produced from strain CLL182 were mixed with strain CMJ534 (*spbK*+) and plated via top agar overlay. **D**) Magnified view of an area from **(B)** containing different plaque morphologies. SP β -like plaques (small and cloudy) could be distinguished from $\Phi 3T$ plaques (large and clear) visually. Arrows indicate typical plaque morphologies of SP β and $\Phi 3T$. **E**) Genome comparisons of SP β c2 (top; yellow), $\Phi \beta$ phages ($\Phi 3T$ -SP β hybrids) (middle), and $\Phi 3T$ (bottom; green). Genomes of hybrid phage lysogens were sequenced and annotated. Prophage sequences were manually extracted from the genome and aligned with clinker [57]. Regions from $\Phi 3T$ are indicated in green and those from SP β c2 in yellow. The counter-defense gene *nip* (*phi3T_120*) is between the two vertical lines and indicated at the bottom. **F**) *Nip* is necessary and sufficient for evading SpbK-mediated phage defense. Ten-fold dilutions of $\Phi 3T \Delta nip$ were spotted onto isogenic strains without anti-phage defense (CU1050; top row), expressing *spbK* (CMJ534; middle row), or co-expressing *spbK* and *nip* (CLL356; bottom row). Large zones of clearing are indicative of a confluence of phage plaques and cell lysis. Small zones of clearing are indicative of individual or small clusters of phage plaques. **G**) Expression of *nip* restores plating efficiency of $\Phi 3T \Delta nip$ on strains expressing *spbK*. $\Phi 3T$ was plated with isogenic strains expressing no anti-phage defense (CU1050, top bar), *spbK* (CMJ534, middle bar), or *spbK* and *nip* together (CLL356, bottom bar). Error bars represent standard deviation and are not always visible due to the size of the data point. **H**) Expression of *nip* prevents SpbK-mediated inhibition of SP β . Ten-fold dilutions of SP β were spotted onto isogenic strains without anti-phage defense (CU1050; top row), expressing *spbK* (CMJ534; middle row), or co-expressing *spbK* and *nip* (CLL356; bottom row). Large zones of clearing are indicative of a confluence of phage plaques and cell lysis. Small zones of clearing are indicative of individual or small clusters of phage plaques. **I**) Expression of *nip* restores plating efficiency of SP β on strains expressing *spbK*. SP β was plated with isogenic strains expressing no anti-phage defense (CU1050, top bar), *spbK* (CMJ534, middle bar), or *spbK* and *nip* together (CLL356, bottom bar). Data shown for no defense and *spbK* are from Fig 1F and shown here for comparison. The limit of detection in these experiments was $\sim 10^5$ PFU/ml. Error bars represent standard deviation and are not always visible due to the size of the data point.

<https://doi.org/10.1371/journal.pgen.1011551.g003>

although we have no other indication of this. Together, these results indicate that SpbK interacts with YonE, and that the YonE(A291P) mutant that is functional for phage production has reduced interaction with SpbK.

We found that an N-terminal fragment of SpbK was sufficient to interact with YonE. We fused the N-terminal 115 amino acids of SpbK, including the N-terminal domain and linker region (Fig 1A) but not the TIR domain, to the N-terminus of GFP (SpbK(1–115)-GFP) and expressed this allele in cells with YonE-Myc. We immunoprecipitated with anti-GFP antibodies and found that YonE-Myc co-precipitated (Fig 2E, lane 4), indicating this region of SpbK directly interacts with YonE. As controls, we expressed SpbK(1–115)-GFP with wild type YonE (no tag) (Fig 2E, lane 2) and the N-terminal region of SpbK without a GFP tag with YonE-Myc (Fig 2E, lane 3). As above, we detected YonE-Myc in input samples, and detection of YonE-Myc in the immunoprecipitates was dependent on expression of SpbK(1–115)-GFP. Similar to results expressing FLAG-SpbK and YonE(A291P)-Myc, we did not observe an interaction between SpbK(1–115)-GFP and YonE(A291P)-Myc (Fig 2E, lane 5). Because the TIR (NADase) domain was no longer present, co-expression of SpbK(1–115) or SpbK(1–115)-GFP did not cause growth arrest. Further, SpbK(1–115) and SpbK(1–115)-GFP was not sufficient to inhibit production of SP β following infection (S2A Fig), indicating that this interaction alone was not sufficient to block phage production.

We compared AlphaFold3 [15] predictions to our experimental observations of interaction between YonE and SpbK (Fig 2F–2H). The YonE(A291P) mutation is predicted with high confidence to be in the clip domain (Fig 3F). The clip domain of portal proteins interacts with the large terminase and plug proteins during DNA packaging and helps stabilize the phage tail [16], and YonE-like portal proteins form dodecamers [8]. Due to the current limitations of the AlphaFold3 server, we were unable to model the complete dodecameric structure of the portal with an equivalent number of SpbK monomers. Therefore, we modeled six YonE monomers with six SpbK monomers (Fig 2G and 2H). AlphaFold3 predicted, with low confidence, that the N-terminal region of SpbK interacts with the clip domain of YonE, with the interface located near A291 (Fig 2G and 2H). The low confidence of the

model indicates that the molecular details of the known interaction are likely not accurate, perhaps due to limitations on the oligomeric inputs. Nonetheless, the experimental results (Fig 2A and 2E) are quite clear about interactions between the N-terminal domain of SpbK and YonE and the role of the clip domain in those interactions. Oligomerization of TIR domains is often a prerequisite for NADase activity [17–19]. Thus, we suspect that localization of the N-terminal region of SpbK to the clip domain of YonE facilitates oligomerization of the TIR domains and opening of the NAD binding pocket, as has been observed for other TIR-domain-containing NADases [20]. Overall, our results are most consistent with the conclusion that the N-terminal region of SpbK interacts with the clip domain of YonE, and this interaction leads to oligomerization and activation of SpbK, and subsequent depletion of NAD⁺.

Phage Φ3T encodes a counter-defense against SpbK

We tested the ability of SpbK to protect against the phages Φ3T and ρ11, both closely related to SPβ [21,22]. Both Φ3T and ρ11 were able to grow and make plaques with similar efficiencies on strains with and without *spbK* (Figs 3A, 3B, S3A and S3B), indicating that both phages were resistant to SpbK-mediated defense. It was possible that resistance of these two phages to SpbK was caused by a mutation in *yonE*, analogous to the mutant we isolated above. However, we found that the sequence of *yonE* from each phage was identical at the nucleotide sequence level to that of *yonE* from SPβ. Thus, we suspected that Φ3T and ρ11 might encode a counter-defense that prevented SpbK from functioning in abortive infection.

Φ3T- SPβ hybrid phages. To identify the possible counter-defense gene(s), we made hybrid phages, each of which had some genes from SPβ and some from Φ3T. To do this, we isolated SPβ-like hybrids that were able to evade SpbK-mediated defense. Briefly, we constructed a double lysogen that harbored both Φ3T and a temperature sensitive mutant of SPβ, SPβc2 [23]. Since ρ11 contains the same attachment site as SPβ at *spsM* [21,24] and Φ3T integrates at *kamA* [21], we focused on Φ3T since we could easily construct a double lysogen. From the double lysogen, we induced the temperature sensitive SPβc2 with heat shock. The population of phages coming from the double lysogen should include SPβc2 and Φ3T, and some recombinants between the two phages. We screened this mixed population of phages for those that had the small, turbid plaque morphology of SPβ (in contrast to the much larger plaques formed by Φ3T) but were able to grow and make plaques on cells expressing *spbK* (Fig 3C and 3D). We isolated 10 independent hybrid phages (named Φβ1 - Φβ10), verified the phenotypes, and then sequenced and compared their genomes (Fig 3E).

There were two genes from Φ3T, *phi3T_120* and *phi3T_121* that were present in all 10 hybrid phages (Fig 4E). We changed the third codon of *phi3T_121* from a lysine to a stop codon{Φ3T *phi3T_121*(K3*)}. We found that this mutant was virtually indistinguishable from wild type Φ3T in its resistance to SpbK-mediated defense (S3C and S3D Fig), indicating that *phi3T_121* was not needed for counter-defense. We therefore focused on *phi3T_120*.

***phi3T_120* (*nip*) is required for counter-defense.** We found that deletion *phi3T_120* (Φ3T Δ*phi3T_120*) caused a >10³-fold drop in plaquing efficiency on cells expressing *spbK* (Fig 3F and 3G), indicating that *phi3T_120* (now named *nip*, for NADase inhibitor from phage) was required for Φ3T to overcome SpbK-mediated defense and productively grow on cells expressing *spbK*. ρ11 has a gene that is identical to *nip* (*phi3T_120*) from Φ3T. We deleted *nip* from ρ11 (ρ11 Δ*nip*) and found that this mutant phage was now sensitive to SpbK-mediated defense. That is, ρ11 Δ*nip* had decreased efficiency of plating on cells expressing *spbK* (S3E and S3F Fig). Together, these results show that *nip* provides Φ3T and ρ11 with counter-defense against SpbK.

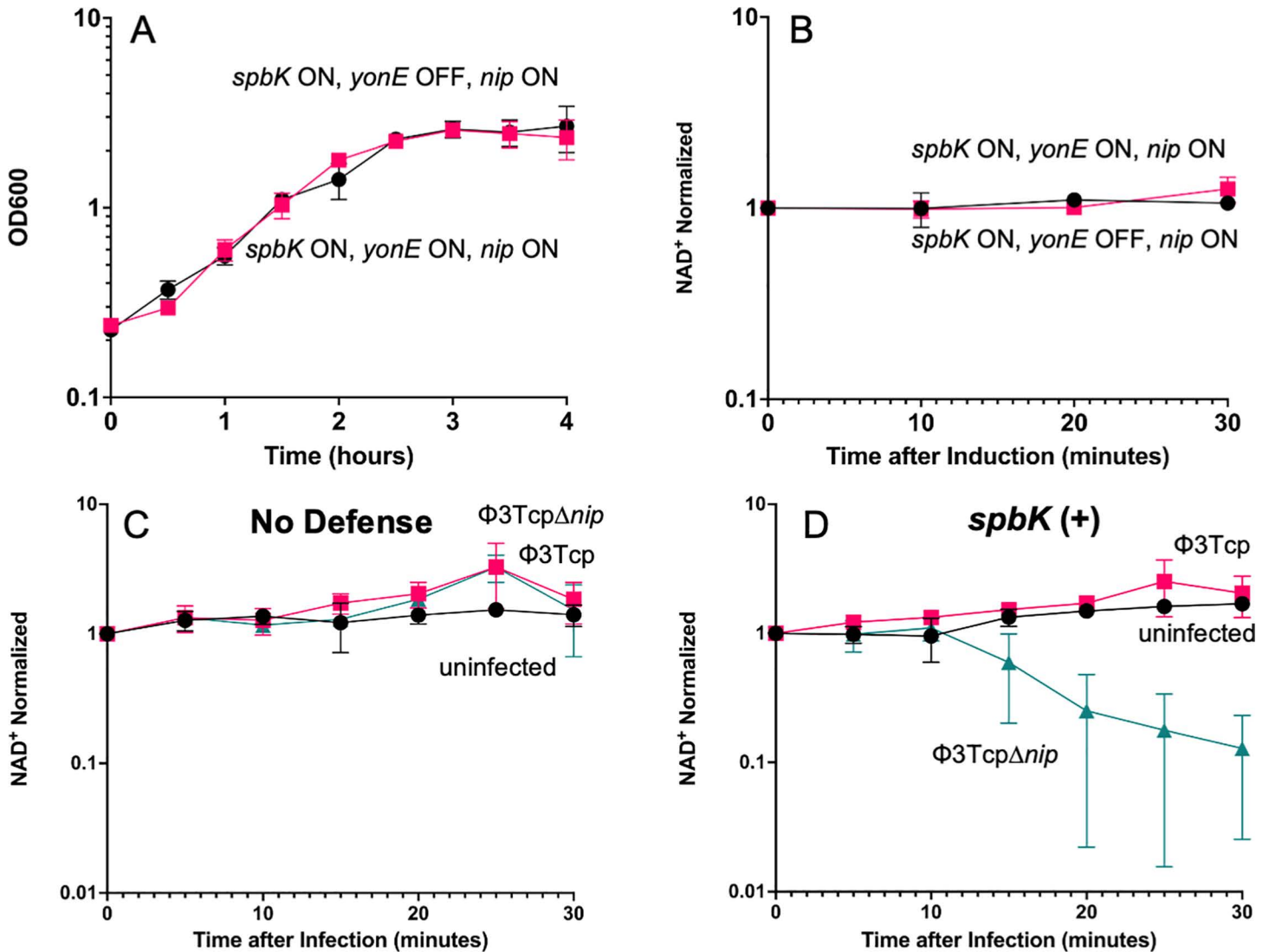


Fig 4. Expression of *nip* prevents growth arrest and NAD⁺ depletion during phage infection. A, B) Expression of *nip* prevents growth arrest (A) and depletion of intracellular levels of NAD⁺ (B) when strains are also expressing *spbK* and *yonE*. Culture turbidity by OD600 (A) and intracellular levels of NAD⁺ (B) were measured and followed over time in strains co-expressing *spbK*, *yonE*, and *nip* (CLL353; black circles) or strains co-expressing *spbK* and *nip*, with uninduced *yonE* (CLL353; pink squares) in *S*₇₀ minimal medium. Expression of *yonE* was induced by addition of 1mM IPTG. Data represent three biological replicates. Error bars represent standard deviation and are not always depicted due to the size of the data point. C, D) *nip* prevents depletion of NAD⁺ in cells during phage infection. Strains without phage defense (PY79) (C) or expressing *spbK* (CMJ684) (D) were infected with Φ 3T_{tcp} (pink squares), Φ 3T_{tcp} Δ *nip* (turquoise triangles), or left uninfected (black circles). Levels of NAD⁺ were measured and followed over time. Samples at T=0 were taken immediately before infection. Phages were added at a multiplicity of infection of 10 in infected samples. Data shown represent three biological replicates. Error bars represent standard deviation and are not always depicted due to the size of the data point.

<https://doi.org/10.1371/journal.pgen.1011551.g004>

***phi3T_120* (*nip*) is sufficient for counter-defense.** We cloned *nip* under control of the constitutive promoter Ppen (Ppen-*nip*) and integrated this in the *B. subtilis* chromosome. Φ 3T Δ *nip* was able to grow and make plaques on cells that were expressing both *spbK* and *nip* (Fig 3F and 3G), in contrast to the reduced plaquing efficiency on cells expressing only *spbK* (Fig 3F and 3G). These results indicate that Ppen-*nip* is functional and that Δ *nip* in Φ 3T is not polar.

We found that SP β was also able to grow and make plaques on cells that were expressing both *nip* (Ppen-*nip*) and *spbK* (Fig 3H and 3I), in contrast to the reduced plaquing efficiency

on cells expressing only *spbK* (Figs 1G, 1H, 3H, and 3I). Based on these results, we conclude that *nip* is a counter-defense gene that confers resistance to SpbK-mediated defense, that *nip* (*phi3T_120*) is required for Φ 3T to evade SpbK-mediated defense, and that *nip* is the only gene in Φ 3T needed to confer this counter-defense to SP β .

Predicted structure and conservation of Nip. We used HHpred and DALI to identify proteins with structures related to that predicted for Nip, and AlphaFold3 to predict the structure of a Nip monomer. Nip is predicted to have two SH3-like domains in its N-terminal region and a dimerization domain similar to that from the bacterial nucleoid-associated protein HU in its C-terminal region (S4A and S4B Fig) [14,25]. Additionally, we used PSI-BLAST to search for *nip* homologues and found that *nip*-like genes were primarily conserved in the genus *Bacillus* (S1 Table). We expect many of these homologues are in temperate phages.

Based on the phenotypes of *nip*, we suspected that it would interact with SpbK and/or YonE. However, using AlphaFold3, there were no models for interactions with any reasonable level of confidence, likely because of little sequence identity of Nip to proteins with known structures, its low conservation outside of *Bacillus* species, and perhaps the inability to model large multimeric structures.

Nip inhibits the NADase activity of SpbK

Because *nip* allowed Φ 3T, ρ 11, and SP β to escape SpbK-mediated abortive infection, we suspected that it would inhibit the YonE-activated NADase activity of SpbK. We expressed *nip* (Ppen-*nip*) in the absence of any phage genes, other than *yonE*, in cells expressing *spbK* and *yonE* (Fig 4A). The growth of cells expressing all three genes was indistinguishable from that of cells expressing only *spbK* (Fig 4A). Additionally, there was no detectable drop in levels of NAD⁺ in cells expressing all three genes (*nip*, *spbK*, and *yonE*) (Fig 4B). These results are in marked contrast to the effects of expressing *spbK* and *yonE* in the absence of *nip* (Fig 1C) and indicate that *nip* was functional outside the context of phage infection and was sufficient to inhibit the NADase activity of SpbK and to confer counter-defense.

We also found that *nip* functions to inhibit the NADase activity of SpbK during phage infection. As described above, infection of *spbK*-expressing cells with Φ 3T resulted in phage growth and eventual cell lysis, leading to the release of functional phage. We found no detectable drop in levels of NAD⁺ when cells expressing *spbK* were infected with a clear plaque mutant of Φ 3T (Φ 3T_{cp}) which can only undergo lytic growth and cannot enter the lysogenic cycle (Fig 4C). In contrast, there was an approximate 10-fold drop in levels of NAD⁺ when *spbK*-expressing cells were infected by Φ 3T_{cp} Δ *nip* (Fig 4D). Based on these results, we conclude that *nip* is a counter-defense gene in Φ 3T (and ρ 11) that is both necessary and sufficient for inhibiting the NADase activity of SpbK and enabling productive phage growth in cells with the SpbK abortive infection system.

Nip binds to SpbK and forms a tripartite complex with YonE

There are a few different ways in which Nip could directly affect the NADase activity of SpbK. Nip might interact directly with YonE and prevent it from interacting with SpbK. Nip might instead interact with SpbK and prevent it from interacting with YonE. In this model, Nip would likely interact with the N-terminal domain of SpbK (the region that interacts with YonE). Alternatively, Nip might interact with the C-terminal TIR domain of SpbK and inhibit NADase activity. This interaction might or might not prevent interactions between SpbK and YonE.

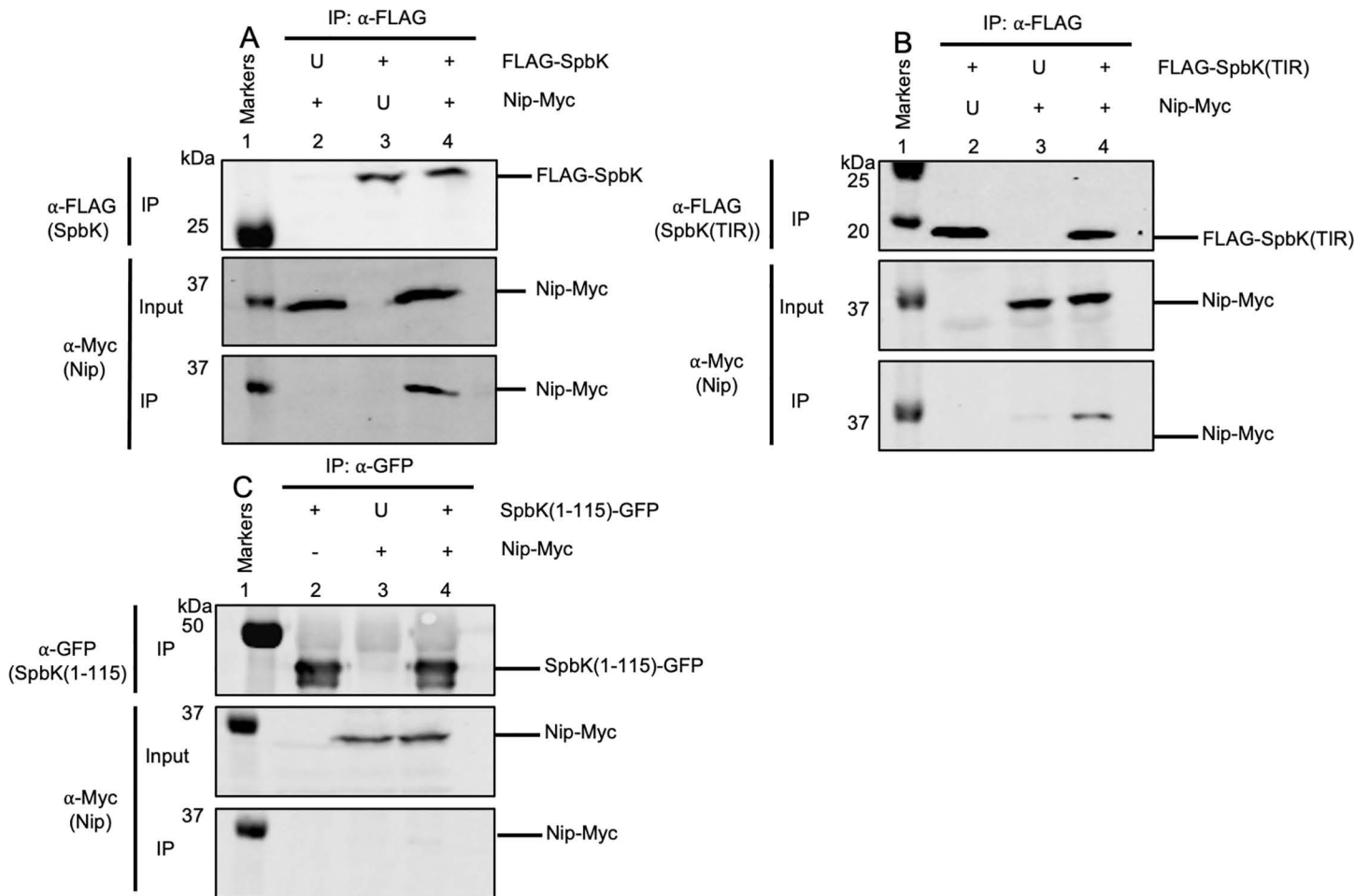


Fig 5. Nip interacts with the TIR domain of SpbK. Indicated proteins were produced in cells without *ICEBs1* or *SP β* . In each panel, lane 1 contains molecular weight markers from the Odyssey One-Color Protein Molecular Weight Marker Ladder (LI-COR). U, untagged protein expressed; +, tagged protein expressed; -, protein not expressed. **(A)** SpbK interacts with Nip. Monoclonal α -FLAG antibodies were used to immunoprecipitate FLAG-SpbK. Western blots were probed with α -FLAG monoclonal antibodies (top panel) or α -c-Myc monoclonal antibodies (bottom two panels). Top row: Western blot probed with α -FLAG monoclonal antibody on immunoprecipitated fractions. Second row: Western blot probed with α -c-Myc monoclonal antibody on input fractions. Third row: Western blot probed with α -c-Myc monoclonal antibody on IP fractions. Lysates from the following strains were used for immunoprecipitations: CLL388 (lane 2), CLL390 (lane 3), and CLL376 (lane 4). Data shown are representative of three biological replicates. **(B)** Nip interacts with the TIR domain of SpbK. Monoclonal α -FLAG antibodies were used to immunoprecipitate FLAG-SpbK. Top row: Western blot probed with α -FLAG monoclonal antibody on immunoprecipitated fractions. Second row: Western blot probed with α -c-Myc monoclonal antibody on input fractions. Third row: Western blot probed with α -c-Myc monoclonal antibody on immunoprecipitated fractions. Lysates from the following strains were used for immunoprecipitations: CLL669 (lane 2), CLL671 (lane 3), and CLL670 (lane 4). Data shown are representative of three biological replicates. **(C)** No interaction was detected between Nip and the N-terminal domain of SpbK. Polyclonal α -GFP antibodies were used to immunoprecipitate SpbK(1-115)-GFP. Top row: Western blot probed with α -GFP polyclonal antibody on immunoprecipitated fractions. Second row: Western blot probed with α -c-Myc monoclonal antibody on input fractions. Third row: Western blot probed with α -c-Myc monoclonal antibody on immunoprecipitated fractions. Lysates from the following strains were used for immunoprecipitations: CLL726 (lane 2), CLL725 (lane 3), and CLL727 (lane 4). Data shown are representative of three biological replicates.

<https://doi.org/10.1371/journal.pgen.1011551.g005>

To distinguish between these models, we used epitope-tagged proteins (described below) to test directly for interactions between Nip, SpbK, and YonE, in the absence of any other phage or *ICEBs1* genes. Experiments described below demonstrate that Nip interacts with the C-terminal domain of SpbK and that YonE, SpbK, and Nip can form a tripartite complex.

Direct interaction between Nip and SpbK. We found that Nip interacts with SpbK. We fused a 3xMyc tag to the C-terminus of Nip (Nip-Myc). Nip-Myc was functional in preventing SpbK-mediated defense against SP β (S2A Fig). We immunoprecipitated

FLAG-SpbK using anti-FLAG antibodies from cells co-expressing Nip-Myc and found that Nip-Myc co-immunoprecipitated (Fig 5A, lane 4), indicating that Nip and SpbK interact. In control experiments in which we expressed wild type SpbK (no tag) with Nip-Myc or FLAG-SpbK with wild type Nip (no tag) we no longer detected Nip-Myc in Western blots of immunoprecipitated material (Fig 5A, lanes 2 and 3), indicating the antibodies used in the immunoprecipitation and Western blot were specific to the tagged proteins and not cross-reacting with the other protein of interest.

Nip interacts with the C-terminal NADase/TIR domain of SpbK. We found that Nip interacts with the C-terminal part of SpbK that contains the TIR domain. We fused the FLAG tag to the N-terminus of the linker and TIR domain (aa 95–276) of SpbK {FLAG-SpbK(TIR)} and precipitated with anti-FLAG antibodies, as with full length FLAG-SpbK above. We found that Nip-Myc co-immunoprecipitated with FLAG-SpbK(TIR) (Fig 5B, lane 4). As controls, we expressed FLAG-SpbK(TIR) with wild type Nip (no tag) (Fig 5B, lane 2) or SpbK(TIR) (no tag) with Nip-Myc (Fig 5B, lane 3) and did not observe an interaction. Nip-Myc was detected in in cell extracts (Fig 5B, lanes 3 and 4) and only detected in immunoprecipitates when FLAG-SpbK(TIR) was also present (Fig 5B, lane 4).

We also tested for the ability of Nip to interact with the N-terminal region of SpbK. We immunoprecipitated the SpbK(1–115)-GFP fusion protein with anti-GFP antibodies and did not detect coprecipitation of Nip in cells also expressing Nip-Myc (Fig 5C, lane 4). Similar to controls in previous experiments, we expressed SpbK(115)-GFP with wild type Nip (no tag) (Fig 5C, lane 2) and SpbK(1–115) (no tag) with Nip-Myc (Fig 5C, lane 3) and did not observe an interaction. Together, the results from the immunoprecipitation experiments indicate that Nip interacts with the TIR domain and not the N-terminal region of SpbK.

Nip forms a tripartite complex with SpbK and YonE. We found that Nip, SpbK, and YonE coprecipitate (Figs 6 and S5). Using cells expressing Nip-GFP, FLAG-SpbK, and YonE-Myc, we immunoprecipitated Nip-GFP and found that both FLAG-SpbK and YonE-Myc were in the immunoprecipitates (Fig 6, lane 5). The presence of FLAG-SpbK and YonE-Myc

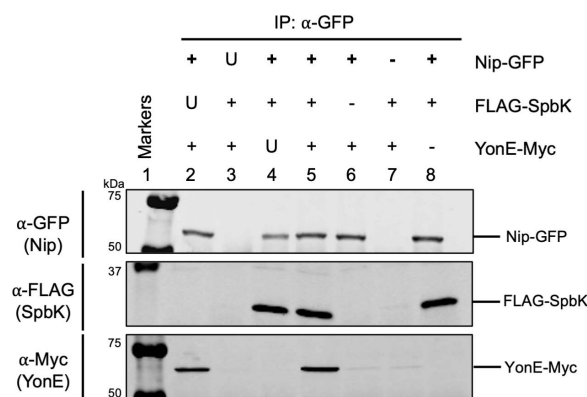


Fig 6. Nip, SpbK, and YonE form a tripartite complex. Indicated proteins were produced in cells without ICEBs1 or SPβ. α-GFP antibodies were used to immunoprecipitate Nip-GFP. Top row: Western blot probed with α-GFP polyclonal antibody on immunoprecipitated fractions. Second row: Western blot probed with α-FLAG monoclonal antibody on immunoprecipitated fractions. Third row: Western blot probed with α-c-Myc monoclonal antibody on immunoprecipitated fractions. The ladder in lane 1 is composed of molecular weight markers from the Odyssey One-Color Protein Molecular Weight Marker Ladder (LI-COR). Lysates from the following strains were used for immunoprecipitations: CLL633 (lane 2), CLL642 (lane 3), and CLL704 (lane 4), CLL498 (lane 5), CLL497 (lane 6), CLL373 (lane 7), and CLL382 (lane 8). Data shown are representative of three biological replicates. U, untagged protein expressed; +, tagged protein expressed; -, protein not expressed.

<https://doi.org/10.1371/journal.pgen.1011551.g006>

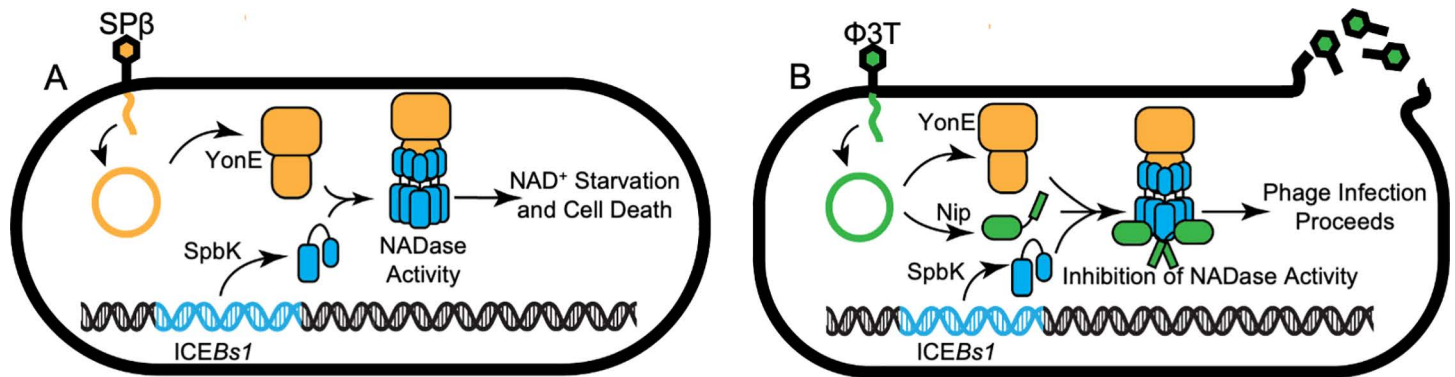


Fig 7. Model for activation and inhibition of the NADase SpbK. The simplest model based on data presented is that the indicated proteins interact directly. We cannot rule out a possible role for one or more host proteins, but there is no evidence for this. The model includes YonE as a multimer (portal proteins are typically dodecamers [8]) and SpbK oligomerizing and becoming active as an NADase by binding to the YonE oligomer. **A**) Model of SpbK-mediated anti-phage defense. SPβ phage adsorbs to the host cell and injects its DNA (orange) into the cell. Phage portal YonE (orange shapes) is produced during lytic phage infection. ICEBs1 (light blue) is an integrative and conjugative element found in the chromosome of *B. subtilis*. The ICEBs1-encoded protein SpbK (light blue cylinders) associates with YonE and leading to activation of the SpbK NADase activity, NAD⁺ depletion, and cell death. **B**) Model of Nip-mediated counter-defense. The SPβ-like phage Φ3T (green) adsorbs to the cell and extrudes its DNA (green) into the cell. During lytic infection, Φ3T expresses YonE and a counter defense protein, Nip (green), that binds to SpbK (light blue) and inhibits SpbK-mediated NADase activity, resulting in phage production.

<https://doi.org/10.1371/journal.pgen.1011551.g007>

was specific as we detected little or none of either of these proteins in the immunoprecipitates from cells expressing Nip without the GFP tag (Fig 6, lane 3). Both proteins were present in the cell extracts prior to immunoprecipitation (S5 Fig). Additionally, the antibodies used in the Western blots were specific for each of the tagged proteins as there was no signal if the protein did not contain the epitope tag (Fig 6, lane 2, no FLAG; lane 4, no Myc).

Co-precipitation of Spbk and YonE with Nip could indicate separate bipartite interactions: Nip with SpbK, as described above (Fig 6), and Nip with YonE. If so, then coprecipitation of YonE with Nip would be independent of the presence of SpbK, as the coprecipitation of Nip and SpbK is independent of YonE (Fig 6). Alternatively, the coprecipitation of YonE with Nip could reflect the presence of a tripartite complex containing YonE, SpbK, and Nip. In this scenario, coprecipitation of YonE with Nip would depend on the presence of SpbK.

We found that Nip, SpbK, and YonE form a tripartite complex. YonE-Myc was not coprecipitated with Nip-GFP in cells that were not also producing SpbK (Fig 6, lane 6). The presence of either FLAG-SpbK (Fig 6, lane 5) or the native untagged SpbK (Fig 6, lane 2) was required for coprecipitation of YonE-Myc with Nip-GFP. Together, these results indicate that Nip, SpbK, and YonE can form a tripartite complex (Fig 6), that interactions between Nip and SpbK are independent of YonE (Fig 5), and interactions between SpbK and YonE are independent of Nip (Fig 2).

In total, the simplest interpretation of our results is that the clip domain of the phage portal protein YonE interacts with the N-terminal domain of the ICEBs1-encoded protein SpbK. This interaction stimulates the NADase activity of SpbK, leading to a drop in intracellular levels of NAD⁺, cell death [5], and the inability of phage to grow and make plaques (Fig 7A). Phages that encode the counter-defense protein Nip (or when Nip is ectopically expressed) escape the SpbK-mediated defense because Nip binds to the TIR domain of SpbK and inhibits NADase activity and abortive infection (Fig 7B).

Discussion

Work presented here shows that the anti-phage defense protein SpbK, encoded by ICEBs1, is an NADase that is activated by the essential phage portal protein YonE, encoded by the temperate phage SPβ and its relatives, including phages Φ3T and ρ11 (Fig 7A). We identified

a counter-defense gene, *nip*, found in $\Phi 3T$ and $\rho 11$. *Nip* interacts directly with the TIR domain of SpbK to inhibit NADase activity (Fig 7B). Below we discuss the presence of anti-phage defense genes on mobile genetic elements, the types of phage products that are often involved in activating defense systems, the role of NAD⁺ in anti-phage defense, and the roles of phage-encoded counter-defense genes.

Anti-phage defense genes on mobile genetic elements

Anti-phage defense systems are often found on mobile genetic elements [26,27] that facilitate rapid acquisition and dissemination of these accessory genes. The presence of defense genes between conserved core element genes [28,29] likely facilitates recombination between similar elements, increasing genetic diversity within bacterial populations. Additionally, many analyses that utilize ectopic overexpression of an anti-phage defense system and infection by lytic phages [30–32] have also found defense systems that are found naturally on mobile genetic elements.

Although bacteria are threatened by infection with lytic phages, nearly half of sequenced bacteria contain temperate phages, either integrated into the chromosome or maintained as a plasmid [33–35]. These temperate phages co-evolve with their hosts and with the other mobile elements, including other phages, plasmids, and ICEs, that reside in the same host. Discovery and analyses of systems from temperate phages and their co-resident mobile elements should reveal how their co-existence and co-evolution affect the properties of these elements and their defense and counter-defense systems.

Phage products that activate anti-phage defense systems

Anti-phage systems that work through abortive infection are inactive until phage infection is recognized. The triggers for abortive infection are often conserved phage-encoded proteins that are essential for the phage lifecycle. For example, the phage portal protein (YonE in the case of SP β) is essential for phage growth. Most mutations in an essential phage gene would prevent phage growth (beneficial for the bacterium), which makes it a suitable target for detecting phage infection. The low frequency ($\sim 10^{-10}$) with which we found the SP β *yonE*(A291P) mutant that escapes SpbK-mediated defense is likely due to the fitness tradeoffs imposed on the phage when both the function as a phage portal and escaping anti-phage defense are required of YonE. The frequency of phages acquiring new genes is likely greater than the relatively low frequency of mutations that allow escape from defense and maintain full function for phage growth. This is likely the reason that some phages in the SP β family have a counter-defense gene rather than an alteration in *yonE* to prevent SpbK-mediated abortive infection.

Role of NAD⁺ in anti-phage defense

Anti-phage defense systems that halt cell growth and/or cause cell death target essential host functions. NAD⁺ is required in all known living organisms and is the target of several anti-phage defense systems. For example, the Thoeris anti-phage system has a TIR-domain-containing protein, ThsB, that generates a signaling molecule that activates ThsA, a protein with a SIR2 domain, that then depletes NAD⁺ in infected cells [10,30]. Some of the cyclic-oligonucleotide-based anti-phage signaling systems (CBASS) also contain TIR domains with NADase activity [36,37]. Some prokaryotic Argonaute systems contain TIR domains that cause depletion of NAD⁺ when foreign DNA is present in cells [38]. TIR domain-containing proteins are widespread and play important roles in regulating cell death in both prokaryotes and eukaryotes [9].

Phage-encoded counter-defense systems

Several different phage-encoded counter-defense systems counteract the effects of anti-phage systems that have NADases. For example, Tad1 and Tad2 inhibit Thoeris-mediated anti-phage defense by sequestering the signaling molecules produced by Thoeris during infection, thus preventing activation of the Thoeris-encoded NADase [2,39]. Another strategy is to replenish NAD⁺ levels during phage infection after an NADase effector from an anti-phage defense has been activated. The NARP1 and NARP2 counter-defense systems work in this way [40]. Notably, the NARP1 system is encoded by an SP β -like phage that does not contain *nip*, however the gene for NARP1 and Nip are in different locations in the related phages [40]. Thus, related phages have two different mechanisms of counteracting NADase mediated defense: replenish NAD levels (NARP1) and directly bind and inhibit the NADase (Nip).

nip is in a region of Φ 3T that is expressed early (based on analyses of SP β), in contrast to *yonE* which is expressed late during phage infection [41]. Expression of *nip* before *yonE* likely provides sufficient time for Nip to bind and inactivate the TIR (NADase) domain of SpbK before YonE is expressed. The operon containing *nip* encodes another counter-defense, Gad1, which inhibits Gabija anti-phage defense [2]. Other phages and mobile genetic elements have counter-defense genes that are genetically linked and cluster near one another. For example, phage T4 genes *tifA* and *dmd* are in an operon and each confers resistance to toxin-antitoxin systems [42,43]. Anti-CRISPRs, one of the most diverse types of counter-defense proteins, can be found clustered near one another on both phages and conjugative elements [44]. Some plasmids have been discovered to harbor counter-defense genes in the leading region of conjugative elements [45]. Similarly to anti-phage defense hotspots, it appears that there are hotspots in phages and other mobile genetic elements for the accommodation of counter-defense genes, and these are often located in operons that are expressed early during phage infection (or conjugative transfer), likely to inhibit defense systems prior to or concomitant with expression of the activator protein.

Materials and methods

Media and growth conditions

B. subtilis cells were grown in LB or S7₅₀ minimal medium supplemented with 0.1% glutamate and 1% glucose as a carbon source [46]. *E. coli* was grown in LB medium and on LB agar plates (1.5% bacto-agar). Isopropyl β -D-1-thiogalactopyranoside (IPTG) was used at 1 mM to induce expression from the LacI-repressible IPTG-inducible promoter Pspank(hy). Antibiotics used for selection in *B. subtilis* included: kanamycin (5 μ g/ml), spectinomycin (100 μ g/ml), chloramphenicol (5 μ g/ml), tetracycline (10 μ g/ml), and erythromycin (0.5 μ g/ml) plus lincomycin (12.5 μ g/ml) for macrolide-lincosamide-streptogramin (MLS) resistance.

For typical experiments, a culture was started from a single colony (after overnight growth) and grown at 37°C to mid-late exponential phase in the indicated medium. Cells were diluted into fresh medium for continued growth as indicated. For experiments with genes expressed from an inducible promoter, cultures were split at the time of dilution into medium with and without inducer, as indicated.

Temperate phages were induced by addition of mitomycin C (MMC) to 1 μ g/ml to a lysogen growing exponentially in LB medium at 37°C. After MMC induction, cells were grown for one additional hour and pelleted at 4000g for 5 minutes in a tabletop centrifuge. The lysate was transferred to a new tube, 1:100 v/v chloroform was added to inhibit cell growth, and stored at 4°C.

Efficiency of plating. Phage stocks were diluted in phage buffer (150 mM NaCl, 40 mM Tris-Cl, 10 mM MgSO₄) and mixed with 300 μ l of cells that were growing exponentially in

Table 1. *B. subtilis* strains used.

Strain	Genotype [reference]
CLL118	PY79; SPβ ⁺ ICEBsI ⁰
CLL136	ρ11 ⁺ , BGSC 1L27; DBS-15(rho11)
CLL152	PY79; Φ3T
CLL156	PY79; <i>lacA</i> ::{ <i>spbK</i> (E192Q) <i>kan</i> }
CLL164	CU1050; <i>lacA</i> ::{ <i>spbK</i> (E192Q) <i>kan</i> }
CLL191	CU1050; SPβ-Φ3T Hybrid 1 (Φβ1)
CLL192	CU1050; SPβ-Φ3T Hybrid 2 (Φβ2)
CLL196	CU1050; SPβ-Φ3T Hybrid 7 (Φβ7)
CLL203	CU1050; SPβ-Φ3T Hybrid 5 (Φβ5)
CLL204	CU1050; SPβ-Φ3T Hybrid 8 (Φβ8)
CLL205	CU1050; SPβ-Φ3T Hybrid 4 (Φβ4)
CLL216	CU1050; SPβ-Φ3T Hybrid 3 (Φβ3)
CLL217	CU1050; SPβ-Φ3T Hybrid 9 (Φβ9)
CLL221	CU1050; SPβ-Φ3T Hybrid 6 (Φβ6)
CLL222	CU1050; SPβ-Φ3T Hybrid 10 (Φβ10)
CLL265	PY79; <i>amyE</i> ::{Ppen- <i>nip</i> -3xmyc <i>cat</i> }
CLL273	PY79; Φ3T Δ <i>nipT</i>
CLL317	PY79; <i>lacA</i> ::{ <i>spbK</i> (E192Q) <i>kan</i> } <i>amyE</i> ::{Pspank(hy)- <i>yonE lacI spc</i> }
CLL322	PY79; ρ11 ⁺ Δ <i>nipT</i>
CLL328	PY79; <i>amyE</i> ::{Pspank(hy)- <i>yonE</i> -3xmyc} <i>lacI spc</i> }
CLL334	PY79; <i>lacA</i> ::{ <i>spbK kan</i> } <i>amyE</i> ::{Pspank(hy)- <i>yonE</i> -3xmyc <i>lacI spc</i> }
CLL337	PY79; <i>cgeD</i> ::{Ppen- <i>nip tet</i> }
CLL353	PY79; <i>lacA</i> ::{ <i>spbK kan</i> } <i>amyE</i> ::{Pspank(hy)- <i>yonE lacI spc</i> } <i>cgeD</i> ::{Ppen- <i>nip tet</i> }
CLL356	CU1050; <i>lacA</i> ::{ <i>spbK kan</i> } <i>cgeD</i> ::{Ppen- <i>nip tet</i> }
CLL370	PY79; <i>cgeD</i> ::{Ppen- <i>nip-gfp tet</i> }
CLL373	PY79; <i>lacA</i> ::{ <i>flag-spbK kan</i> } <i>amyE</i> ::{Pspank(hy)- <i>yonE</i> -3xmyc <i>lacI spc</i> }
CLL376	PY79; <i>lacA</i> ::{ <i>flag-spbK kan</i> } <i>amyE</i> ::{Ppen- <i>nip</i> -3xmyc <i>cat</i> }
CLL382	PY79; <i>lacA</i> ::{ <i>flag-spbK kan</i> } <i>cgeD</i> ::{Ppen- <i>nip-gfp tet</i> }
CLL388	PY79; <i>lacA</i> ::{ <i>spbK kan</i> } <i>amyE</i> ::{Ppen- <i>nip</i> -3xmyc <i>cat</i> }
CLL390	PY79; <i>cgeD</i> ::{Ppen- <i>nip tet</i> } <i>lacA</i> ::{ <i>flag-spbK kan</i> }
CLL395	PY79; <i>lacA</i> ::{ <i>spbK kan</i> } <i>amyE</i> ::{Pspank(hy)- <i>yonE</i> (A291P) <i>lacI spec</i> }
CLL445	JMA222; SPβ(<i>yonE</i> (A291P) <i>trpC2 pheA1</i> ICEBsI ⁰)
CLL452	PY79; SPβ ⁺ ICEBsI ⁰ , <i>lacA</i> ::{ <i>spbK kan</i> }
CLL453	PY79; SPβ <i>yonE</i> (A291P) ICEBsI ⁰
CLL466	PY79; SPβ <i>yonE</i> (A291P) ICEBsI ⁰ , <i>lacA</i> ::{ <i>spbK kan</i> }
CLL497	PY79; <i>amyE</i> ::{Pspank(hy)- <i>yonE</i> -3xmyc <i>lacI spc</i> } <i>cgeD</i> ::{Ppen- <i>nip-gfp tet</i> }
CLL498	PY79; <i>lacA</i> ::{ <i>flag-spbK kan</i> } <i>amyE</i> ::{Pspank(hy)- <i>yonE</i> -3xmyc <i>lacI spc</i> } <i>cgeD</i> ::{Ppen- <i>nip-gfp tet</i> }
CLL600	PY79; <i>amyE</i> ::{Pspank(hy)- <i>yonE</i> (A291P) <i>lacI spc</i> }
CLL609	PY79; <i>lacA</i> ::{ <i>flag-spbK</i> } <i>amyE</i> ::{Pspank(hy)- <i>yonE lacI spc</i> }
CLL615	PY79; <i>amyE</i> ::{Pspank(hy)- <i>yonE</i> (A291P)-3xmyc <i>lacI spc</i> } <i>lacA</i> ::{ <i>flag-spbK kan</i> }
CLL633	PY79; <i>amyE</i> ::{Pspank(hy)- <i>yonE</i> -3xmyc <i>lacI spc</i> } <i>cgeD</i> ::{Ppen- <i>nip-gfp tet</i> } <i>lacA</i> ::{ <i>spbK kan</i> }
CLL642	PY79; <i>lacA</i> ::{ <i>flag-spbK kan</i> } <i>amyE</i> ::{Pspank(hy)- <i>yonE</i> -3xmyc <i>lacI spc</i> } <i>cgeD</i> ::{Ppen- <i>nip tet</i> }
CLL673	PY79; <i>cgeD</i> ::{Ppen- <i>nip</i> -3xmyc <i>tet</i> }
CLL681	PY79; <i>lacA</i> ::{ <i>flag-spbK</i> (TIR) <i>kan</i> } <i>cgeD</i> ::{Ppen- <i>nip tet</i> }
CLL682	PY79; <i>lacA</i> ::{ <i>spbK</i> (TIR) <i>kan</i> } <i>cgeD</i> ::{Ppen- <i>nip-gfp tet</i> }

(Continued)

Table 1. (Continued)

Strain	Genotype [reference]
CLL683	PY79; <i>lacA</i> ::{ <i>flag-spbK(TIR) kan</i> } <i>cgeD</i> ::{Ppen- <i>nip-gfp tet</i> }
CLL704	PY79; <i>amyE</i> ::{Pspank(hy)- <i>yonE lacI spc</i> } <i>cgeD</i> ::{Ppen- <i>nip-gfp tet</i> } <i>lacA</i> ::{ <i>flag-spbK kan</i> }
CLL716	PY79; <i>lacA</i> ::{ <i>spbK(1-115) kan</i> }
CLL717	PY79; <i>lacA</i> ::{ <i>spbK(1-115)-gfp kan</i> }
CLL718	PY79; <i>lacA</i> ::{ <i>spbK(1-115) kan</i> } <i>amyE</i> ::{Pspank(hy)- <i>yonE-3xmyc lacI spc</i> }
CLL719	PY79; <i>lacA</i> ::{ <i>spbK(1-115)-gfp kan</i> } <i>amyE</i> ::{Pspank(hy)- <i>yonE lacI spc</i> }
CLL720	PY79; <i>lacA</i> ::{ <i>spbK(1-115)-gfp kan</i> } <i>amyE</i> ::{Pspank(hy)- <i>yonE-3xmyc lacI spc</i> }
CLL721	PY79; <i>lacA</i> ::{ <i>spbK(1-115)-gfp kan</i> } <i>amyE</i> ::{Pspank(hy)- <i>yonE(A291P)-3xmyc lacI spc</i> }
CLL725	PY79; <i>lacA</i> ::{ <i>spbK(1-115) kan</i> } <i>cgeD</i> ::{Ppen- <i>nip-3xmyc tet</i> }
CLL726	PY79; <i>lacA</i> ::{ <i>spbK(1-115)-gfp kan</i> } <i>cgeD</i> ::{Ppen- <i>nip tet</i> }
CLL727	PY79; <i>lacA</i> ::{ <i>spbK(1-115)-gfp kan</i> } <i>cgeD</i> ::{Ppen- <i>nip-3xmyc tet</i> }
CLL728	CU1050; <i>lacA</i> ::{ <i>spbK(1-115) kan</i> }
CLL729	CU1050; <i>lacA</i> ::{ <i>spbK(1-115)-gfp kan</i> }
CMJ534	CU1050; <i>lacA</i> ::{ <i>spbK kan</i> } [5]
CMJ582	PY79; <i>lacA</i> ::{ <i>flag-spbK kan</i> }
CMJ616	PY79; <i>amyE</i> ::{Pspank(hy)- <i>yonE lacI spc</i> } [5]
CMJ684	PY79; <i>lacA</i> ::{ <i>spbK kan</i> } [5]
CMJ685	PY79; <i>lacA</i> ::{ <i>spbK kan</i> } <i>amyE</i> ::{Pspank(hy)- <i>yonE lacI spc</i> } [5]
CU1050	ICEBs1 ⁰ SPβ ⁰ <i>metA thrC leu codY sup-3 (trnS-lys)</i> [5,54]
JMA222	SPβ ⁺ <i>trpC2 pheA1 ICEBs1⁰</i> [55]
PY79	SPβ ⁰ ICEBs1 ⁰ [56]

<https://doi.org/10.1371/journal.pgen.1011551.t001>

LB medium. Cells and phage were incubated for 5 minutes at room temperature to allow adsorption, transferred to 3 ml of molten LB + 0.5% bacto-agar, and plated onto warm LB agar plates. Plates were incubated at 30°C overnight to allow plaque formation.

Serial dilutions (typically 10-fold) for spot assays were made in phage buffer and 2 μl were spotted onto a lawn of cells on LB agar plates. Phage plaquing efficiencies were determined essentially as described [5]. Briefly, 100 μl of various dilutions of a phage stock were mixed with 300 μl of cells that had been grown to OD₆₀₀ of ~0.5 (~3 × 10⁷ cells), incubated at room temperature for 5 minutes, mixed with 3 ml LB top agar and spread onto an LB agar plate. Plaques were counted after incubation overnight at 30°C and are presented at plaque-forming units per ml (PFU/ml) of phage stock.

Cell growth following phage infection. Cells were grown from a single colony in LB medium to OD₆₀₀ ~0.5, and back diluted to OD ~0.05, and 180 μl were added to each well of a 96 well plate and mixed with 20 μl of phage or 20 μl of phage buffer. Plates were incubated at 37°C with shaking in a Biotek Synergy H1 plate reader with OD₆₀₀ measurements taken every 15 minutes.

Strains and alleles

E. coli strain AG1111 (MC1061 F' *lacI^q lacZM15 Tn10*) was used as a host for plasmid cloning. *B. subtilis* strains used are listed in Table 1 and phages used are listed in Table 2. All strains are derivatives of PY79 [47] or CU1050 [48], both of which are cured of SPβ and ICEBs1. Indicated alleles were introduced by natural transformation [49] and appropriate selection. New constructs and alleles are described below.

Table 2. Phages used.

Phage	Genotype, phenotype, description (comment, source, reference)
SPβ	from strain JMA222 [55]
SPβc2	ts mutant of SPβ; temperature-inducible; (phage isolated from BGSC 1A322; CU4142)
SPβcp	Spontaneous clear plaque mutant of SPβ; (this study)
SPβ <i>yonE(A291P)</i>	SPβ mutant that escapes SpbK-mediated defense; in strain CLL445 (this study)
Φ3T	from strain CLL152; {phage isolated from BGSC 1L26; 3610(phi3T)}
Φ3Tcp	Spontaneous clear plaque mutant of Φ3T (this study)
Φ3TΔ <i>nip</i>	From strain CLL273 (this study)
Φ3TcpΔ <i>nip</i>	Spontaneous clear plaque mutant of Φ3TΔ <i>nip</i> ; (this study)
ρ11	from strain CLL136; {phage isolated from BGSC 1L27; DBS-15(rho11)}
ρ11Δ <i>nip</i>	from strain CLL322 (this study)
Φβ1	SPβ-Φ3T hybrid; from strain CLL191 (this study)
Φβ2	SPβ-Φ3T hybrid; from strain CLL192 (this study)
Φβ3	SPβ-Φ3T hybrid; from strain CLL216 (this study)
Φβ4	SPβ-Φ3T hybrid; from strain CLL205 (this study)
Φβ5	SPβ-Φ3T hybrid; from strain CLL203 (this study)
Φβ6	SPβ-Φ3T hybrid; from strain CLL221 (this study)
Φβ7	SPβ-Φ3T hybrid; from strain CLL196 (this study)
Φβ8	SPβ-Φ3T hybrid; from strain CLL204 (this study)
Φβ9	SPβ-Φ3T hybrid; from strain CLL217 (this study)
Φβ10	SPβ-Φ3T hybrid; from strain CLL222 (this study)

<https://doi.org/10.1371/journal.pgen.1011551.t002>

Unmarked deletions were generated by inserting flanking homology regions into pCAL1422 digested with BamHI and EcoRI via Gibson isothermal assembly [50]. pCAL1422 is a plasmid containing *E. coli lacZ* and *cat* (chloramphenicol-resistance in *B. subtilis*) [51]. The assembled plasmids were transformed into *E. coli* strain AG1111. After the correct plasmid construct was verified by PCR and Sanger sequencing, plasmids were transformed into *B. subtilis* selecting for chloramphenicol resistance (indicating an integrated plasmid by single crossover recombination). Transformants were grown in LB liquid medium and plated onto LB plates supplemented with 120 mg/ml X-gal. Colonies were screened for loss of *lacZ* and verified to have the desired deletion by PCR.

Deletion of *nip* from Φ3T. We made a deletion of the Φ3T gene *nip* in a lysogen of Φ3T. The deletion of *nip* extended from the start to stop codons of *nip* and was constructed as described above after cloning DNA flanking the deletion endpoints into the integration vector pCAL1422.

Ectopic expression of *nip*. *cgeD::Ppen-nip* (CLL337) was used to test for inhibition of SpbK-mediated anti-phage defense and growth arrest. *nip* was cloned downstream of the promoter Ppen and the *spoVG* ribosome binding site (Ppen-*nip*) and integrated into the nonessential gene *cgeD*. The 5' fragment was amplified containing the upstream *cgeD* homology arm, tetracycline resistance gene, Ppen, and the *spoVG* ribosome binding site. The 3' fragment contained the downstream *cgeD* homology arm. *nip* from 3 bp upstream of the start codon to 110 bp downstream of the stop codon was amplified by PCR, assembled with the 5' and 3' fragments by Gibson isothermal assembly, and transformed into *B. subtilis*.

Fusions of *nip* to 3xmyc and *gfp*. Constructs expressing *nip* with different epitope tags were used in immunoprecipitation assays. Briefly, gDNA from CLL337 was used to amplify fragments containing *nip*, Ppen promoter, *spoVG* ribosome binding site, and *cgeD* or *amyE* homology arms. DNA encoding the tags was amplified from previously generated constructs

and inserted at the 3' end of *nip* via Gibson isothermal assembly to generate *nip-3xmyc* (CLL265 and CLL673) and *nip-gfp* (CLL370) [50]. The resulting constructs were transformed into *B. subtilis* selecting for tetracycline resistance.

Ectopic expression alleles of *spbK*. Strains expressing *spbK* from its own promoter that had been integrated into *lacA* were previously described [5]. *lacA::{spbK(E192Q) kan}* (CLL156), encoding a catalytically dead mutant of SpbK, was made by amplifying two fragments of *spbK* and surrounding *lacA* sequence (with genomic DNA from CMJ684 [5] as the template), upstream and downstream of the mutation, using overlapping primers that contained the mutation (changing codon 192 from 5'-GAA-3' to 5'-CAA-3'). Fragments were assembled via isothermal assembly and the resulting construct was transformed into *B. subtilis*, selecting for resistance to kanamycin. *lacA::{flag-spbK kan}* (CMJ582), used in immunoprecipitation assays, was constructed by Chris Johnson. It consists of a *flag* tag inserted directly after the start codon of *spbK*.

Ectopic expression alleles of *yonE*. *amyE::{Pspank(hy)-yonE spc}* (CMJ616) was previously described [5]. *amyE::{Pspank(hy)-yonE(A291P)}* (CLL380) was made by amplifying a fragment of *yonE(A291P)* from the mutant SP β that was resistant to (escaped) SpbK-mediated defense and inserted into pCAL1422 via Gibson isothermal assembly, essentially as described generally above. The plasmid was crossed into a strain with *amyE::{Pspank(hy)-yonE spc}* (CMJ616) and recombinants that had lost the plasmid were screened by PCR to have the desired *yonE(A291P)* mutation.

amyE::{Pspank(hy)-yonE-3xmyc spc} (CLL328) and *amyE::{Pspank(hy)-yonE(A291P)-3xmyc spc}* (CLL600) were used for co-immunoprecipitation assays. For each allele, a *3xmyc* tag was fused to the 3' end of *yonE*, directly upstream of the stop codon.

Ectopic expression of the N-terminal region of SpbK. *lacA::{spbK(1–115) kan}* (CLL716) was used as a control in immunoprecipitation assays. The 5' end of *spbK* was amplified by PCR. This fragment extends from 330 bp upstream of the start codon to codon 115 and includes the *spbK* promoter and encodes the N-terminal and linker regions of SpbK.

lacA::{spbK(1–115)-gfp kan} (CLL717) was used in immunoprecipitation assays. Fragments were amplified from CLL716 and *gfp* inserted between codon 115 and the stop codon of *spbK*.

Ectopic expression of the TIR domain of SpbK. *lacA::{spbK(TIR) kan}* (CLL662) and *lacA::{flag-spbK(TIR)}* (CLL661) were used in immunoprecipitation assays. The linker and TIR domains (encoded by codons 95–267) were expressed under the endogenous promoter of *spbK*. Fragments were amplified from CMJ582 (*lacA::{flag-spbK kan}*) extending from the 5' *lacA* homology arm to the *flag tag* for the first fragment and extending from codon 95 to the 3' *lacA* homology arm for the second fragment. This construct was transformed into *B. subtilis*, selecting for kanamycin resistance.

Isolation of clear plaque phage mutants. All phages used in this study are temperate and typically develop turbid plaques on susceptible cells. Occasionally, clear plaques are observed, indicative of a mutant that can only undergo lytic growth and cannot enter the lysogenic lifestyle. Clear plaque mutant phages were isolated by picking a spontaneously occurring clear plaque, resuspended in phage buffer, and used to infect cells to allow phage growth. Infected cells were added to top agar (LB + 0.5% agar), plated via double agar overlay method, and incubated overnight. Phage buffer (5 ml) was added to the plates and the cells within top agar were scraped off. The mix was centrifuged and chloroform added to the supernatant (phage stock) to inhibit cell growth. Phage stocks were stored at 4°C.

Lysogens of temperate phages. Cells were plated with phage in top agar (LB + 0.5% agar) to generate turbid phage plaques (indicative of lysogens). Plaques were picked with a toothpick and streaked onto LB plates to isolate single colonies. Strains were confirmed to have the desired phage via PCR.

Generation and sequencing of hybrid phages

Hybrid phages were generated inducing SP β c2- Φ 3T double lysogens with heat shock at 50°C for 20 minutes. Cells were grown for an additional hour at 37°C to allow phage production. Phage lysate containing approximately 10³ PFUs was mixed with 3ml of molten top agar (LB + 0.5% agar), poured onto LB plates, and incubated overnight at 30°C overnight to allow the formation of plaques. Lysogens were isolated from SP β -like plaques and genomic DNA was prepared using the DNeasy Tissue and Blood Kit (Qiagen) and sequenced via Nanopore sequencing on an R9 PromethION flowcell. Genomes were assembled using Flye assembler [52] and annotated using Prokka [53].

Co-immunoprecipitation and Western blotting

Cells were grown in 100 ml LB cultures to OD 0.5-1.0 and 50 OD units of cells were pelleted in conical tubes at 4000g for 10 minutes, washed once with 5 ml of PBS, spun once more at 4000g for 10 minutes, and the supernatant was decanted. The pellet was resuspended in 450 μ l of resuspension buffer (20% sucrose, 50 mM NaCl, 10 mM EDTA, 10 mM Tris-HCl pH 8.0) supplemented with 10 mg/ml lysozyme, 10 μ l of P8849 protease inhibitor cocktail, and 250 units of Benzonase and incubated at 37°C for 15 minutes. 450 μ l of lysis buffer (100 mM Tris-HCl pH 7.0, 300 mM NaCl, 10 mM EDTA, 1% Triton X-100) was used to complete lysis. 30 μ l of protein A beads suspended in ddH₂O (Fisher Scientific, 50% v/v) were used to clear the lysate for non-specific binding proteins. Beads were pelleted, supernatant transferred to a new tube and incubated with appropriate antibody for 30 minutes. Antibodies used to bind the protein A beads include rabbit anti-GFP (Covance) and rabbit anti-FLAG (Cell Signaling Technologies). After incubation with antibody, 60 μ l of protein beads suspended in ddH₂O (Fisher Scientific, 50% v/v) were added and incubated overnight at 4°C to form the immunocomplex. Beads were then washed three times with wash buffer (22.5mM Tris-HCl (pH 8.0), 0.5M Sucrose, 10mM EDTA) supplemented with 1% triton. 2x SDS sample buffer (100 mM Tris-HCl (pH 6.8), 20% glycerol, 4% SDS, 0.02% bromophenol blue) supplemented with 2-mercaptoethanol was added and boiled to elute proteins from the beads. Proteins were separated on a 10% SDS-PAGE and transferred to 0.2 μ m nitrocellulose membrane using the Trans-blot SD semi-dry transfer cell (Bio-Rad). Blots were blocked for one hour with Odyssey Blocking Buffer. Mouse M2 anti-flag (1:1000; Millipore Sigma), rabbit anti-GFP (1:10,000; Covance), or mouse anti-c-Myc (1:500; Thermo Fischer) antibodies were used as primary antibodies. Blots were then washed with PBST (phosphate buffered saline + 0.2% Tween) five times for five minutes. Goat anti-mouse antibodies with a conjugated fluorophore (1:10,000; Avantor/VWR) was used as a secondary antibody. Blots were imaged on a Li-Cor scanner.

Measuring NAD⁺ levels

NAD⁺ was measured using the NAD/NADH-Glo Assay kit (Promega). Cells were grown overnight at 30°C in S7₅₀ minimal medium supplemented with glucose. Starter cultures were grown in S7₅₀ supplemented with glucose at 37°C until OD₆₀₀ 0.5 and diluted into S7₅₀ supplemented with glucose to an OD₆₀₀ of 0.25. Where indicated, regulated promoters were induced by addition of 1 mM IPTG and 5 ml samples were taken every 10 minutes after induction and chilled on ice to stop growth. Cells were pelleted for 5 minutes at 10000g at room temperature on a tabletop centrifuge, supernatant was decanted, and cells were saved at -80°C until processing. Cells were processed following the supplier's protocol.

During phage infection, cells were infected at a multiplicity of infection of 10, harvested every 5 minutes, immediately chilled on ice to stop growth, and spun at 4000g for 5 minutes at room temperature. Cells were processed as above.

Supporting information

S1 Fig. SpbK is structurally similar to proteins with TIR domains that act as NADases.

A, B) An AlphaFold3 model of an SpbK (blue) monomer overlaid with AbTIR (pink; PDB: 7UXU). The NAD molecule is colored yellow. **B)** An enlarged view of the NAD binding pocket from A. **C, D)** An AlphaFold3 model of an SpbK (blue) monomer overlaid with the TIR domain from TIR-APAZ (green; PDB: 8I87). The NAD molecule is colored yellow. **D)** An enlarged view of the NAD binding pocket from C. **E)** Sequence logo of the 500 highest scoring proteins from PSI-BLAST using SpbK as the query. The TIR domain of SpbK (amino acids 115–266) are shown. The highly conserved glutamate in the TIR domain NADases, E192 in SpbK, is marked with an asterisk (*). (TIF)

S2 Fig. Fusion proteins of Nip, SpbK, and YonE are functional. **A)** Fusion proteins Nip-Myc (top row) and Nip-GFP (second row) were co-expressed with wild type SpbK. FLAG-SpbK (third row), SpbK(1–115) (fourth row), and SpbK(1–115)-GFP (fifth row) were expressed alone. Ten-fold dilutions of SP β were spotted and functionality was assessed by observing presence or absence of phage plaques. Large zones of clearing are indicative of a confluence of phage plaques and cell lysis. Small zones of clearing are indicative of individual or small clusters of phage plaques. **B)** YonE-Myc causes growth arrest when co-expressed with wild type SpbK. Strains co-expressing *spbK* and *yonE-3xmyc* were grown in LB medium. Turbidity of the culture was measured by OD₆₀₀ and followed over time when *yonE-3xmyc* was induced with 1mM IPTG (maroon triangles) or left uninduced (purple inverted triangles). Measurements at T=0 were taken immediately before addition of IPTG. Error bars represent standard deviation. Data shown are from three biological replicates. Error bars represent standard deviation and are not always depicted due to the size of the data point. (TIF)

S3 Fig. *nip* is necessary and sufficient to prevent SpbK-mediated phage defense in ρ 11, SP β , and Φ 3T. **A, B)** ρ 11 evades SpbK-mediated anti-phage defense. **A)** Ten-fold dilutions of ρ 11 were spotted onto isogenic strains without phage defense (CU1050, top), expressing *spbK* (CMJ534, middle), or co-expressing *spbK* and *nip* (CLL356; bottom). Large zones of clearing indicate cell lysis while small zones of clearing are indicative of productive phage infection. ρ 11 was plated with isogenic strains expressing no anti-phage defense (CU1050, top bar), *spbK* (CMJ534, middle bar), or *spbK* and *nip* together (CLL356, bottom bar). Error bars represent standard deviation and are not always depicted due to the size of the data point. **C, D)** Φ 3T ϕ hi3T₁₂₁(K3STOP) still has counter-defense against SpbK. **C)** Ten-fold dilutions of Φ 3T ϕ hi3T₁₂₁(K3STOP) were spotted onto isogenic strains lacking anti-phage defense (CU1050, top row) or expressing *spbK* (CMJ534, bottom row). Large zones of clearing indicate cell lysis while small zones of clearing are indicative of productive phage infection. **D)** Strains lacking anti-phage defense (black bar) or expressing *spbK* (pink bar) were infected with Φ 3T ϕ hi3T₁₂₁(K3STOP). Error bars represent standard deviation and are not always visible. **E, F)** *nip* is required for ρ 11 evasion of SpbK-mediated anti-phage defense. **C)** Ten-fold dilutions of ρ 11 Δ *nip* were spotted onto isogenic strains without phage defense (CU1050, top), expressing *spbK* (CMJ534, middle), or co-expressing *spbK* and *nip* (CLL356; bottom). Large zones of clearing indicate cell lysis while small zones of clearing are indicative of productive phage infection. ρ 11 was plated with isogenic strains expressing no anti-phage defense (CU1050, top bar), *spbK* (CMJ534, middle bar), or *spbK* and *nip* together (CLL356, bottom bar). Error bars represent standard deviation and are not always depicted due to the size of the data point. The limit of detection in these experiments was $\sim 10^6$ PFU/ml.

(TIF)

S4 Fig. Predicted domains and structure of the Nip protein. A) Predicted domain architecture of Nip. Amino acid positions are indicated at the top and regions of similarity to other proteins indicated at the bottom. Nip is 279 amino acids and predicted to have two SH3-like domains (purple; aa 33–75 and 112–168) and an HU dimerization-like domain (green; aa 191–268). B) AlphaFold3 model of a monomer of Nip. The SH3-like domains are colored purple and the HU dimerization-like domain is colored green. The pTM score is 0.57 and the mean pLDDT score is 75.62, indicating low-moderate confidence in the model.

(TIF)

S5 Fig. Nip, SpbK, and YonE form a tripartite complex: Input and immunoprecipitation samples. Data for the immunoprecipitation experiments are the same as in Fig 7 and are shown here for comparison. Input samples are shown in the panel above each of the corresponding immunoprecipitations (IP). Indicated proteins were expressed in cells without *ICEBs1* or *SPβ*. First and second rows: Western blots probed with α -GFP polyclonal antibodies on input samples and immunoprecipitates, respectively. Third and fourth rows: Western blot probed with α -FLAG monoclonal antibodies on input samples and immunoprecipitates, respectively. Fifth and sixth rows: Western blot probed with α -c-Myc monoclonal antibodies on input samples and immunoprecipitates, respectively. Lane 1 contains molecular weight markers from the Odyssey One-Color Protein Molecular Weight Marker Ladder (LI-COR). Lysates and IPs were from strains: CLL633 (lane 2), CLL642 (lane 3), and CLL704 (lane 4), CLL498 (lane 5), CLL497 (lane 6), CLL373 (lane 7), and CLL382 (lane 8). Data shown are representative of three biological replicates. U, untagged protein expressed; +, tagged protein expressed; -, protein not expressed.

(TIF)

S1 Table. PSI-BLAST hits for Nip. The excel spreadsheet contains data that resulted from a PSI-BLAST search using the protein sequence of Nip as a query.

(XLSX)

S1 Data. Underlying raw data for experiments presented in graphs. The excel spreadsheet contains the underlying data for the experiments presented in each of the graphs for which the data are not already in the figure.

(XLSX)

Acknowledgments

We thank Stuart Levine and the MIT BioMicro Center for help with genome sequencing, the Bacillus Genetic Stock Center for providing strains, and members of the Grossman Lab for some strains and helpful discussions and Michael Laub, Gene-Wei Li, and Andrew Camilli for useful discussions.

Author contributions

Conceptualization: Christian L. Loyo, Alan D. Grossman.

Funding acquisition: Alan D. Grossman.

Investigation: Christian L. Loyo.

Methodology: Christian L. Loyo, Alan D. Grossman.

Project administration: Christian L. Loyo, Alan D. Grossman.

Supervision: Alan D. Grossman.

Validation: Christian L. Loyo.

Visualization: Christian L. Loyo.

Writing – original draft: Christian L. Loyo.

Writing – review & editing: Christian L. Loyo, Alan D. Grossman.

References

1. Lopatina A, Tal N, Sorek R. Abortive Infection: Bacterial Suicide as an Antiviral Immune Strategy. *Annu Rev Virol.* 2020;7(1):371–84. <https://doi.org/10.1146/annurev-virology-011620-040628> PMID: [32559405](https://pubmed.ncbi.nlm.nih.gov/32559405/)
2. Yirmiya E, Leavitt A, Lu A, Ragucci AE, Avraham C, Osterman I, et al. Phages overcome bacterial immunity via diverse anti-defence proteins. *Nature.* 2024;625(7994):352–9. <https://doi.org/10.1038/s41586-023-06869-w> PMID: [37992756](https://pubmed.ncbi.nlm.nih.gov/37992756/)
3. Hussain FA, Dubert J, Elsherbini J, Murphy M, VanInsberghe D, Arevalo P, et al. Rapid evolutionary turnover of mobile genetic elements drives bacterial resistance to phages. *Science.* 2021;374(6566):488–92. <https://doi.org/10.1126/science.abb1083> PMID: [34672730](https://pubmed.ncbi.nlm.nih.gov/34672730/)
4. Auchtung JM, Aleksanyan N, Bulku A, Berkmen MB. Biology of ICEBs1, an integrative and conjugative element in *Bacillus subtilis*. *Plasmid.* 2016;86:14–25. <https://doi.org/10.1016/j.plasmid.2016.07.001> PMID: [27381852](https://pubmed.ncbi.nlm.nih.gov/27381852/)
5. Johnson CM, Harden MM, Grossman AD. Interactions between mobile genetic elements: An anti-phage gene in an integrative and conjugative element protects host cells from predation by a temperate bacteriophage. *PLoS Genet.* 2022;18(2):e1010065. <https://doi.org/10.1371/journal.pgen.1010065> PMID: [35157704](https://pubmed.ncbi.nlm.nih.gov/35157704/)
6. Johnson CM, Grossman AD. Identification of host genes that affect acquisition of an integrative and conjugative element in *Bacillus subtilis*. *Mol Microbiol.* 2014;93(6):1284–301. <https://doi.org/10.1111/mmi.12736> PMID: [25069588](https://pubmed.ncbi.nlm.nih.gov/25069588/)
7. Cuervo A, Fàbrega-Ferrer M, Machón C, Conesa JJ, Fernández FJ, Pérez-Luque R, et al. Structures of T7 bacteriophage portal and tail suggest a viral DNA retention and ejection mechanism. *Nat Commun.* 2019;10(1):3746. <https://doi.org/10.1038/s41467-019-11705-9> PMID: [31431626](https://pubmed.ncbi.nlm.nih.gov/31431626/)
8. Dedeo CL, Cingolani G, Teschke CM. Portal Protein: The Orchestrator of Capsid Assembly for the dsDNA Tailed Bacteriophages and Herpesviruses. *Annu Rev Virol.* 2019;6(1):141–60. <https://doi.org/10.1146/annurev-virology-092818-015819> PMID: [31337287](https://pubmed.ncbi.nlm.nih.gov/31337287/)
9. Essuman K, Milbrandt J, Dangl JL, Nishimura MT. Shared TIR enzymatic functions regulate cell death and immunity across the tree of life. *Science.* 2022;377(6605):eabo0001. <https://doi.org/10.1126/science.abo0001> PMID: [35857622](https://pubmed.ncbi.nlm.nih.gov/35857622/)
10. Ofir G, Herbst E, Baroz M, Cohen D, Millman A, Doron S, et al. Antiviral activity of bacterial TIR domains via immune signalling molecules. *Nature.* 2021;600(7887):116–20. <https://doi.org/10.1038/s41586-021-04098-7> PMID: [34853457](https://pubmed.ncbi.nlm.nih.gov/34853457/)
11. Essuman K, Summers DW, Sasaki Y, Mao X, Yim AKY, DiAntonio A, et al. TIR Domain Proteins Are an Ancient Family of NAD⁺-Consuming Enzymes. *Curr Biol.* 2018;28(3):421–430.e4. <https://doi.org/10.1016/j.cub.2017.12.024> PMID: [29395922](https://pubmed.ncbi.nlm.nih.gov/29395922/)
12. Wan L, Essuman K, Anderson RG, Sasaki Y, Monteiro F, Chung E-H, et al. TIR domains of plant immune receptors are NAD⁺-cleaving enzymes that promote cell death. *Science.* 2019;365(6455):799–803. <https://doi.org/10.1126/science.aax1771> PMID: [31439793](https://pubmed.ncbi.nlm.nih.gov/31439793/)
13. Wang X, Li X, Yu G, Zhang L, Zhang C, Wang Y, et al. Structural insights into mechanisms of Argonaute protein-associated NADase activation in bacterial immunity. *Cell Res.* 2023;33(9):699–711. <https://doi.org/10.1038/s41422-023-00839-7> PMID: [37311833](https://pubmed.ncbi.nlm.nih.gov/37311833/)
14. Holm L, Laiho A, Törönen P, Salgado M. DALI shines a light on remote homologs: One hundred discoveries. *Protein Sci.* 2023;32(1):e4519. <https://doi.org/10.1002/pro.4519> PMID: [36419248](https://pubmed.ncbi.nlm.nih.gov/36419248/)
15. Abramson J, Adler J, Dunger J, Evans R, Green T, Pritzel A, et al. Accurate structure prediction of biomolecular interactions with AlphaFold 3. *Nature.* 2024;630(8016):493–500. <https://doi.org/10.1038/s41586-024-07487-w> PMID: [38718835](https://pubmed.ncbi.nlm.nih.gov/38718835/)
16. Olia AS, Al-Bassam J, Winn-Stapley DA, Joss L, Casjens SR, Cingolani G. Binding-induced stabilization and assembly of the phage P22 tail accessory factor gp4. *J Mol Biol.* 2006;363(2):558–76. <https://doi.org/10.1016/j.jmb.2006.08.014> PMID: [16970964](https://pubmed.ncbi.nlm.nih.gov/16970964/)

17. Gerdt J, Brace EJ, Sasaki Y, DiAntonio A, Milbrandt J. SARM1 activation triggers axon degeneration locally via NAD⁺ destruction. *Science*. 2015;348(6233):453–7. <https://doi.org/10.1126/science.1258366> PMID: [25908823](https://pubmed.ncbi.nlm.nih.gov/25908823/)
18. Ma S, Lapin D, Liu L, Sun Y, Song W, Zhang X, et al. Direct pathogen-induced assembly of an NLR immune receptor complex to form a holoenzyme. *Science*. 2020;370(6521):eabe3069. <https://doi.org/10.1126/science.abe3069> PMID: [33273071](https://pubmed.ncbi.nlm.nih.gov/33273071/)
19. Martin R, Qi T, Zhang H, Liu F, King M, Toth C, et al. Structure of the activated ROQ1 resistosome directly recognizing the pathogen effector XopQ. *Science*. 2020;370(6521):eabd9993. <https://doi.org/10.1126/science.abd9993> PMID: [33273074](https://pubmed.ncbi.nlm.nih.gov/33273074/)
20. Nimma S, Gu W, Maruta N, Li Y, Pan M, Saikot FK, et al. Structural Evolution of TIR-Domain Signalingosomes. *Front Immunol*. 2021;12:784484. <https://doi.org/10.3389/fimmu.2021.784484> PMID: [34868065](https://pubmed.ncbi.nlm.nih.gov/34868065/)
21. Kohm K, Floccari VA, Lutz VT, Nordmann B, Mittelstädt C, Poehlein A, et al. The Bacillus phage SPβ and its relatives: A temperate phage model system reveals new strains, species, prophage integration loci, conserved proteins and lysogeny management components. 2021. <https://doi.org/10.1101/2021.11.22.469490>
22. Dean DH, Orrego JC, Hutchison KW, Halvorson HO. New temperate bacteriophage for *Bacillus subtilis*, rho 11. *J Virol*. 1976;20(2):509–19. <https://doi.org/10.1128/JVI.20.2.509-519.1976> PMID: [62060](https://pubmed.ncbi.nlm.nih.gov/62060/)
23. Rosenthal R, Toye P, Korman R, Zahler S. The prophage of SPβc2DcitK1, a defective specialized transducing phage of *Bacillus subtilis*. *Genetics*. 1979;92:721–39.
24. Abe K, Kawano Y, Iwamoto K, Arai K, Maruyama Y, Eichenberger P, et al. Developmentally-regulated excision of the SPβ prophage reconstitutes a gene required for spore envelope maturation in *Bacillus subtilis*. *PLoS Genet*. 2014;10(10):e1004636. <https://doi.org/10.1371/journal.pgen.1004636> PMID: [25299644](https://pubmed.ncbi.nlm.nih.gov/25299644/)
25. Zimmermann L, Stephens A, Nam S-Z, Rau D, Kübler J, Lozajic M, et al. A Completely Reimplemented MPI Bioinformatics Toolkit with a New HHpred Server at its Core. *J Mol Biol*. 2018;430(15):2237–43. <https://doi.org/10.1016/j.jmb.2017.12.007> PMID: [29258817](https://pubmed.ncbi.nlm.nih.gov/29258817/)
26. Rocha EPC, Bikard D. Microbial defenses against mobile genetic elements and viruses: Who defends whom from what?. *PLoS Biol*. 2022;20(1):e3001514. <https://doi.org/10.1371/journal.pbio.3001514> PMID: [35025885](https://pubmed.ncbi.nlm.nih.gov/35025885/)
27. Vassallo CN, Doering CR, Littlehale ML, Teodoro GIC, Laub MT. A functional selection reveals previously undetected anti-phage defence systems in the *E. coli* pangenome. *Nat Microbiol*. 2022;7(10):1568–79. <https://doi.org/10.1038/s41564-022-01219-4> PMID: [36123438](https://pubmed.ncbi.nlm.nih.gov/36123438/)
28. Johnson MC, Laderman E, Huiting E, Zhang C, Davidson A, Bondy-Denomy J. Core defense hotspots within *Pseudomonas aeruginosa* are a consistent and rich source of anti-phage defense systems. *Nucleic Acids Res*. 2023;51(10):4995–5005. <https://doi.org/10.1093/nar/gkad317> PMID: [37140042](https://pubmed.ncbi.nlm.nih.gov/37140042/)
29. Rousset F, Depardieu F, Miele S, Dowding J, Laval A-L, Lieberman E, et al. Phages and their satellites encode hotspots of antiviral systems. *Cell Host Microbe*. 2022;30(5):740–753.e5. <https://doi.org/10.1016/j.chom.2022.02.018> PMID: [35316646](https://pubmed.ncbi.nlm.nih.gov/35316646/)
30. Doron S, Melamed S, Ofir G, Leavitt A, Lopatina A, Keren M, et al. Systematic discovery of anti-phage defense systems in the microbial pangenome. *Science*. 2018;359(6379):eaar4120. <https://doi.org/10.1126/science.aar4120> PMID: [29371424](https://pubmed.ncbi.nlm.nih.gov/29371424/)
31. Millman A, Melamed S, Leavitt A, Doron S, Bernheim A, Hör J, et al. An expanded arsenal of immune systems that protect bacteria from phages. *Cell Host Microbe*. 2022;30(11):1556–1569.e5. <https://doi.org/10.1016/j.chom.2022.09.017> PMID: [36302390](https://pubmed.ncbi.nlm.nih.gov/36302390/)
32. Hossain AA, Pigli YZ, Baca CF, Heissel S, Thomas A, Libis VK, et al. DNA glycosylases provide antiviral defence in prokaryotes. *Nature*. 2024;629(8011):410–6. <https://doi.org/10.1038/s41586-024-07329-9> PMID: [38632404](https://pubmed.ncbi.nlm.nih.gov/38632404/)
33. Howard-Varona C, Hargreaves KR, Abedon ST, Sullivan MB. Lysogeny in nature: mechanisms, impact and ecology of temperate phages. *ISME J*. 2017;11(7):1511–20. <https://doi.org/10.1038/ismej.2017.16> PMID: [28291233](https://pubmed.ncbi.nlm.nih.gov/28291233/)
34. Touchon M, Bernheim A, Rocha EP. Genetic and life-history traits associated with the distribution of prophages in bacteria. *ISME J*. 2016;10(11):2744–54. <https://doi.org/10.1038/ismej.2016.47> PMID: [27015004](https://pubmed.ncbi.nlm.nih.gov/27015004/)
35. Mäntynen S, Laanto E, Oksanen HM, Poranen MM, Díaz-Muñoz SL. Black box of phage-bacterium interactions: exploring alternative phage infection strategies. *Open Biol*. 2021;11(9):210188. <https://doi.org/10.1098/rsob.210188> PMID: [34520699](https://pubmed.ncbi.nlm.nih.gov/34520699/)
36. Millman A, Melamed S, Amitai G, Sorek R. Diversity and classification of cyclic-oligonucleotide-based anti-phage signalling systems. *Nat Microbiol*. 2020;5(12):1608–15. <https://doi.org/10.1038/s41564-020-0777-y> PMID: [32839535](https://pubmed.ncbi.nlm.nih.gov/32839535/)

37. Hogrel G, Guild A, Graham S, Rickman H, Grünschow S, Bertrand Q, et al. Cyclic nucleotide-induced helical structure activates a TIR immune effector. *Nature*. 2022;608(7924):808–12. <https://doi.org/10.1038/s41586-022-05070-9> PMID: [35948638](https://pubmed.ncbi.nlm.nih.gov/35948638/)
38. Koopal B, Potocnik A, Mutte SK, Aparicio-Maldonado C, Lindhoud S, Vervoort JJM, et al. Short prokaryotic Argonaute systems trigger cell death upon detection of invading DNA. *Cell*. 2022;185(9):1471–1486.e19. <https://doi.org/10.1016/j.cell.2022.03.012> PMID: [35381200](https://pubmed.ncbi.nlm.nih.gov/35381200/)
39. Leavitt A, Yirmiya E, Amitai G, Lu A, Garb J, Herbst E, et al. Viruses inhibit TIR gcADPR signalling to overcome bacterial defence. *Nature*. 2022;611(7935):326–31. <https://doi.org/10.1038/s41586-022-05375-9> PMID: [36174646](https://pubmed.ncbi.nlm.nih.gov/36174646/)
40. Osterman I, Samra H, Rousset F, Loseva E, Itkin M, Malitsky S, et al. Phages reconstitute NAD⁺ to counter bacterial immunity. *Nature*. 2024;634(8036):1160–7. <https://doi.org/10.1038/s41586-024-07986-w> PMID: [39322677](https://pubmed.ncbi.nlm.nih.gov/39322677/)
41. Kohm K, Hertel R. The life cycle of SPβ and related phages. *Arch Virol*. 2021;166(8):2119–30. <https://doi.org/10.1007/s00705-021-05116-9> PMID: [34100162](https://pubmed.ncbi.nlm.nih.gov/34100162/)
42. Srikant S, Guegler CK, Laub MT. The evolution of a counter-defense mechanism in a virus constrains its host range. *Elife*. 2022;11:e79549. <https://doi.org/10.7554/eLife.79549> PMID: [35924892](https://pubmed.ncbi.nlm.nih.gov/35924892/)
43. Otsuka Y, Yonesaki T. Dmd of bacteriophage T4 functions as an antitoxin against *Escherichia coli* LsoA and RnIA toxins. *Mol Microbiol*. 2012;83(4):669–81. <https://doi.org/10.1111/j.1365-2958.2012.07975.x> PMID: [22403819](https://pubmed.ncbi.nlm.nih.gov/22403819/)
44. Pinilla-Redondo R, Shehreen S, Marino ND, Fagerlund RD, Brown CM, Sørensen SJ, et al. Discovery of multiple anti-CRISPRs highlights anti-defence gene clustering in mobile genetic elements. *Nat Commun*. 2020;11(1):5652. <https://doi.org/10.1038/s41467-020-19415-3> PMID: [33159058](https://pubmed.ncbi.nlm.nih.gov/33159058/)
45. Samuel B, Mittelman K, Croitoru SY, Ben Haim M, Burstein D. Diverse anti-defence systems are encoded in the leading region of plasmids. *Nature*. 2024;635(8037):186–92. <https://doi.org/10.1038/s41586-024-07994-w> PMID: [39385022](https://pubmed.ncbi.nlm.nih.gov/39385022/)
46. Jaacks KJ, Healy J, Losick R, Grossman AD. Identification and characterization of genes controlled by the sporulation-regulatory gene *spo0H* in *Bacillus subtilis*. *J Bacteriol*. 1989;171(8):4121–9. <https://doi.org/10.1128/jb.171.8.4121-4129.1989> PMID: [2502532](https://pubmed.ncbi.nlm.nih.gov/2502532/)
47. Schroeder JW, Simmons LA. Complete Genome Sequence of *Bacillus subtilis* Strain PY79. *Genome Announc*. 2013;1(6):e01085–13. <https://doi.org/10.1128/genomeA.01085-13> PMID: [24356846](https://pubmed.ncbi.nlm.nih.gov/24356846/)
48. Johnson CM, Grossman AD. Complete Genome Sequence of *Bacillus subtilis* Strain CU1050, Which Is Sensitive to Phage SPβ. *Genome Announc*. 2016;4(2):e00262–16. <https://doi.org/10.1128/genomeA.00262-16> PMID: [27056236](https://pubmed.ncbi.nlm.nih.gov/27056236/)
49. Harwood C, Cutting S. *Molecular biological methods for Bacillus*. Wiley; 1991. Available from: <https://books.google.com/books?id=-thiQgAACAAJ>
50. Gibson DG, Young L, Chuang R-Y, Venter JC, Hutchison CA III, Smith HO. Enzymatic assembly of DNA molecules up to several hundred kilobases. *Nat Methods*. 2009;6(5):343–5. <https://doi.org/10.1038/nmeth.1318>
51. Thomas J, Lee CA, Grossman AD. A conserved helicase processivity factor is needed for conjugation and replication of an integrative and conjugative element. *PLoS Genet*. 2013;9(1):e1003198. <https://doi.org/10.1371/journal.pgen.1003198> PMID: [23326247](https://pubmed.ncbi.nlm.nih.gov/23326247/)
52. Kolmogorov M, Yuan J, Lin Y, Pevzner PA. Assembly of long, error-prone reads using repeat graphs. *Nat Biotechnol*. 2019;37(5):540–6. <https://doi.org/10.1038/s41587-019-0072-8> PMID: [30936562](https://pubmed.ncbi.nlm.nih.gov/30936562/)
53. Seemann T. Prokka: rapid prokaryotic genome annotation. *Bioinformatics*. 2014;30(14):2068–9. <https://doi.org/10.1093/bioinformatics/btu153> PMID: [24642063](https://pubmed.ncbi.nlm.nih.gov/24642063/)
54. Georgopoulos CP. Suppressor system in *Bacillus subtilis* 168. *J Bacteriol*. 1969;97(3):1397–402. <https://doi.org/10.1128/jb.97.3.1397-1402.1969> PMID: [4975748](https://pubmed.ncbi.nlm.nih.gov/4975748/)
55. Auchtung JM, Lee CA, Monson RE, Lehman AP, Grossman AD. Regulation of a *Bacillus subtilis* mobile genetic element by intercellular signaling and the global DNA damage response. *Proc Natl Acad Sci U S A*. 2005;102(35):12554–9. <https://doi.org/10.1073/pnas.0505835102> PMID: [16105942](https://pubmed.ncbi.nlm.nih.gov/16105942/)
56. Youngman P, Perkins JB, Losick R. Construction of a cloning site near one end of Tn917 into which foreign DNA may be inserted without affecting transposition in *Bacillus subtilis* or expression of the transposon-borne *erm* gene. *Plasmid*. 1984;12(1):1–9. [https://doi.org/10.1016/0147-619x\(84\)90061-1](https://doi.org/10.1016/0147-619x(84)90061-1) PMID: [6093169](https://pubmed.ncbi.nlm.nih.gov/6093169/)
57. Gilchrist CLM, Booth TJ, van Wersch B, van Grieken L, Medema MH, Chooi Y-H. cblaster: a remote search tool for rapid identification and visualization of homologous gene clusters. *Bioinform Adv*. 2021;1(1):vbab016. <https://doi.org/10.1093/bioadv/vbab016> PMID: [36700093](https://pubmed.ncbi.nlm.nih.gov/36700093/)